Synthesis of Carbon Nanotubes on Metallic Grids for Applications in Electrochemical Capacitors

A Thesis by Deniz Nasuhoglu

Department of Chemical Engineering
McGill University

Under the Supervision of

Prof. D. Berk
&
Prof. J-L. Meunier

A thesis submitted to the Faculty of Graduate Studies and Research of McGill University in partial fulfillment of the requirements of the degree of Masters of Engineering

Your file Votre référence
ISBN: 978-0-494-51471-9
Our file Notre référence
ISBN: 978-0-494-51471-9

ABSTRACT

Recently, there has been a growing demand for electrode materials to serve as electrochemical capacitors (EC). It has been an important issue to come up with environment friendly electric power sources to reduce pollution caused by combustion engines of automotive systems. Even though conventional battery systems and fuel cells supply high energy, they lack the high specific power that would be required for hybrid power sources. The ECs can fill the gap between conventional capacitors and batteries.

Carbon nanotubes (CNTs), discovered by Iijima in 1991, attracted great attention in recent years for their unique properties, such as mesoporous character, excellent conductivity, moderate to high specific surface area as well as chemical and mechanical stability. These properties of CNTs make them useful in a wide of range applications including electrode materials for EC applications.

The preparation of CNT electrodes is accomplished by either pasting them onto metallic current collectors with the use of binder materials such as PVDF or growing them from deposited metal nanoparticles on substrates such as graphite paper. The deposition of metal nanoparticles is achieved via sputtering techniques or lengthy electrochemical deposition methods. The aim of this research was to simplify the preparation step by growing CNTs directly on metallic substrates and to study the relationship between surface area and electrochemical capacitance of CNTs. CNTs were produced on metal-alloy grids via chemical vapor deposition (CVD) of acetylene (C_2H_2). The physical characterization of the samples was achieved by Field Emission Scanning Electron Microscopy (FE-SEM), Raman spectroscopy and Single point BET surface area. The electrochemical performance of the samples was evaluated by cyclic voltammetry (CV) in a three electrode electrochemical cell with 1M sulfuric acid (H_2SO_4) solution as the electrolyte.

RÉSUMÉ

Il est devenu important de proposer des sources d'énergie écologiquement acceptables afin de réduire la pollution causée par les moteurs à combustion interne. Bien que les batteries conventionnelles ainsi que les piles à combustible puissent fournir une grande quantité d'énergie, elles ne peuvent fournir la haute puissance nécessaire dans les sources d'énergie hybrides. Les condensateurs électrochimiques (EC) peuvent combler le vide séparant les condensateurs conventionnels et les batteries. La demande pour de nouveaux matériaux d'électrodes à haute surface spécifique devant servir dans les EC est l'intérêt principal qui motive la présente recherche.

Les nanotubes de carbone (CNT)découverts par Iijima en 1991, ont généré un grand intérêt ces dernières années en raison de leurs propriétés intéressantes telles que leur porosité, leur excellente conductivité, leur surface spécifique élevée ainsi que leur stabilité mécanique et chimique. Ces propriétés les rendent utiles dans une grande variété d'applications incluant les matériaux d'électrodes pour les EC.

La préparation d'électrodes de CNT est faite soit en les mélangeant à une pâte appliquée sur des supports métalliques à l'aide de matériaux liants tels que le PVDF, soit en les faisant croître à partir de nanoparticules métalliques sur des substrats tels que le papier de graphite. La déposition de ces particules se fait par des techniques de déposition en phase gazeuse ou par de lentes méthodes électrochimiques. Le but de la présente recherche est de simplifier l'étape de préparation en faisant croître les CNT directement sur des substrats métalliques et d'étudier la relation entre la surface spécifique et la capacité électrochimique des CNT. Ces derniers furent produits sur des grilles d'alliages métalliques par la déposition chimique en phase gazeuse (CVD) de l'acétylène (C_2H_2). La caractérisation des échantillons a été effectuée grâce à la microscopie électronique à balayage (FE-SEM), la spectroscopie Raman et la technique à point unique BET pour la surface spécifique. Les performances électrochimiques des échantillons ont été évaluées par la voltamétrie cyclique (CV) dans une cellule électrochimique à trois électrodes contenant une solution d'acide sulfurique (H_2SO_4) ayant une concentration de 1 M.

ACKNOWLEDGEMENTS

First of all I am thankful to my supervisors Prof. Dimitrios Berk and Prof. Jean_Luc Meunier for giving me the opportunity to work on this project and for their support, precious guidance and encouragement.

I owe a big thank you to Prof. Sasha Omanivic for letting me use his electrochemical equipment as well as his invaluable advice on analysing my results.

I am privileged to have worked with Frank Caporuscio, Lou Cusmich, Gerald Lepkyj, Ranjan Roy and Alain Gagnon who were always available to provide their technical expertise and opinions.

I would like to thank Helen Campbell for all her help with the FE-SEM, Lakshminarayana Rao and Faysal Fadlallah for their time, and booking the FE-SEM.

I wish to express my gratitude to Carole Baddour, Ramona Turcu, Andrew Carkner, Robert Delatolla for helping in and out of the laboratory and Martin Dionne for French translations.

I am grateful to have met Nadia Sabri , who cheered me up whenever I felt down and was extremely understanding and supporting during the stressful times close to the end of my work.

This work was financially supported by the Natural Sciences and Engineering Research Council (NSERC) to whom a big thank you goes and to McGill University who without their help this work would not have been accomplished.

The last but not least, I would like to thank all my family and friends, especially my mother, for their continuous encouragement and support.

TABLE OF CONTENTS

LIST OF FIGURES

LIST OF TABLES

LIST OF ABBREVIATIONS

CNT	Carbon Nanotube
MWNT	Multi-walled Carbon Nanotube
SWNT	Single-walled Carbon Nanotube
CNF	Carbon Nanofiber
FESEM	Field Emission Scanning Electron Microscopy
HRTEM	High Resolution Transmission Electron Microscopy
EC	Electrochemical capacitor
SC	Supercapacitor
C	Capacitance (F)
CV	Cyclic Voltammetry
C_{spec}	Specific capacitance (F/g)
ν	Scan rate (mV/s)
I_c	Capacitive current (mA)
I_{spec}	Specific capacitive current (mA/g)
ENiCu	Electroless Nickel plated Copper
Nich	Nichrome, 40 x 40 mesh sized grid
SS304-40	Stainless steel grade 304, 40 x 40 mesh sized grid
SS304-400	Stainless steel grade 304, 400 x 400 mesh sized grid
CNT-Nich	Carbon Nanotubes synthesized on Nichrome grid
CNT-SS304-40	Carbon Nanotubes synthesized on stainless steel 40 x 40 grid
CNT-SS304-400	Carbon Nanotubes synthesized on stainless steel 400 x 400 grid

Chapter 1 : INTRODUCTION

1.1 Introduction and Problem Description

Carbon Nanotubes (CNTs) discovered by Iijima, attracted great attention in the recent years for their unique properties, such as mesoporous character, excellent conductivity, high specific surface area as well as chemical and mechanical stability. These properties of CNTs make them useful in wide range applications such as nanoscale electronic devices, support for catalysts, hydrogen and energy storage.

Among the energy storage applications, supercapacitors or electrochemical capacitors gained considerable interest in recent years for their higher power densities and higher cycle lives than conventional batteries. Supercapacitors have potential applications in electrical vehicles, portable computers, cellular devices and nano-electronics. Carbons with very high specific surface area such as activated carbon are often used as electrode materials. Activated carbons have very high specific surface area, however a large portion of this surface area lies in the micropores, which are not accessible to ions, therefore not contributing to capacitance.

CNTs with their previously mentioned properties are recognized as a potential electrode material for supercapacitors. The current research is mainly focused on producing well-controlled nanostructure and surface functionality in order to enhance the capacitance and cycleability of the supercapacitors. Two main methods are employed currently to construct CNT electrodes. The first one involves the preparation of electrodes by collecting or purchasing CNTs as powders and pasting them on metallic current collectors trough the use of binding materials such as PVDF. The second method deals with depositing nanoparticles of metal catalysts on substrates such as silicone wafer or graphite paper and growing carbon nanotubes from those sites. These metallic catalysts are usually deposited by either a sputtering technique or lengthy chemical / electrochemical methods which are costly and troublesome. Therefore, it is desirable to

find a method to directly grow CNTs on metallic current collectors with minimum pretreatments. This would eliminate the reduction of electrochemical properties of electrodes due to presence of binding materials and would induce stronger attachment of CNT to the metallic current collector.

The challenge is to find or modify a metal so that it would enable CNT growth. The common metal catalysts used for CNT growth are iron, nickel and cobalt. For this reason it was decided to either use alloys containing nickel and iron or deposit nickel particles on copper to grow CNTs in a thermal chemical vapor deposition reactor (CVD).

This thesis presents the characterization of CNTs produced on electroless nickel plated copper, nichrome and stainless steel grade 304 metallic grids trough electron microscopy, Raman spectroscopy , surface area and electrochemical capacitance measurements.

*1.2 **Project Objectives***

The overall objectives of this research are given below:

1. To synthesize composites based on CNTs to be potentially used as electrochemical capacitors
2. To study the relationship between surface area of CNTs and electrochemical capacitance

*1.3 **Thesis Outline***

This thesis is divided into five chapters. A brief description of the organization of each chapter is given below:

Chapter 1: Introduction

This chapter contains the introduction and the problem description along with a list of the project objectives.

Chapter 2: Literature review

The literature review chapter is divided into five sections. In the first section an introduction to carbon materials and CNTs is given. The second section deals with the properties of CNTs. The third section includes the common synthesis methods for CNTs. The fourth section gives a general idea about the mechanism of formation and growth of CNTs. Finally, the fifth section introduces the characterization methods employed in this master's thesis along with detailed literature review on research groups investigating electrochemical properties of CNTs.

Chapter 3: Experimental Materials and Methods

This chapter includes the design of the experimental setup, the detailed experimental procedure, and details on equipment and setups used for characterization of carbon.

Chapter 4: Results and Discussions

In this chapter, the results obtained by FESEM, Raman spectroscopy, BET single point surface area and cyclic voltammetry of prepared CNTs on metallic grids are presented and discussed.

Chapter 5: Conclusions and recommendations

This chapter summarizes the overall conclusions related to the research, including sources of errors and ways of improving them. Finally, recommendations on areas to be studied to improve the results obtained are given.

A list of references is found at the end of the thesis.

Chapter 2 : LITERATURE REVIEW

2.1 Overview of Carbon Structures and Nanotubes

2.1.1 Background on Carbon Structures

The electronic configuration of the carbon atom ($1s^2\ 2s^2p^2$) allows it to form four different chemical bonds around it. The molecular geometry and properties of various types of carbon structures depend on the type of hybridization of carbon atoms. Carbon structures may contain a sp^1, sp^2, sp^3 or a mix of these hybridizations. Among the various possible crystalline structures possible for carbon materials the most common ones are graphite, diamond, fullerenes (or buckyballs), carbon nanotubes (CNT). During the synthesis of these materials amorphous carbon may also be produced which lack a specific crystalline structure. Figure 2.1 below shows the arrangement of carbon atoms in the mentioned carbon materials.

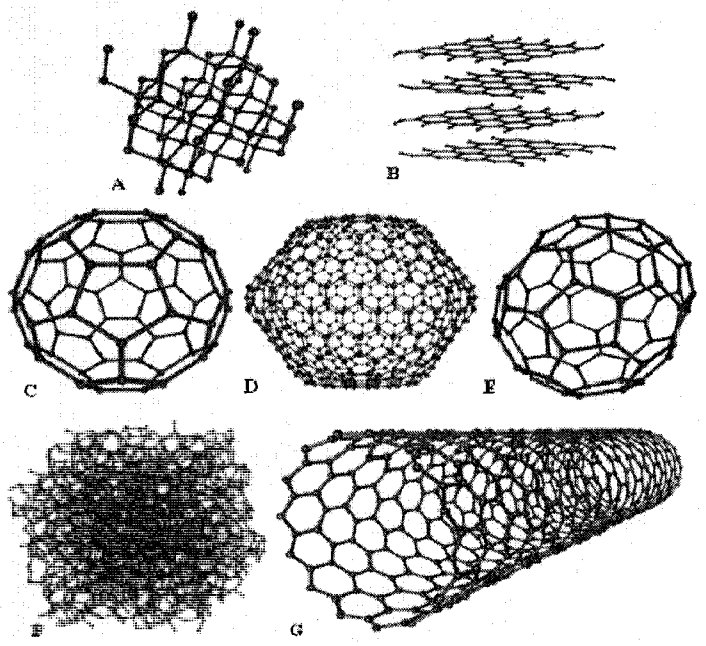

Figure2.1: Arrangements of carbon atoms in various types of carbon materials A-Diamond B- Graphite C,D,E - Fullerenes of C-60, C-540, C-70 F-Amorphous carbon G-Carbon Nanotube

Graphite contains parallel sheets composed of 2-D network of sp^2 hybridized carbon atoms assembled in a honeycomb like structure (i.e. hexagons of carbon atoms) as seen in in Figure 2.1 A. These sheets are called graphene. The high conductivity of graphite is attributed to the fact that the graphene sheet contains free pi (π) electrons which are shared with neighbouring carbon atoms. The sheets are held together by weak Van der Waals forces which give graphene sheets the ability to slide over each other. This aspect of graphite makes it to be easily machineable and have good lubricative properties. Other interesting physical properties of graphite involve high tensile strength and modulus of elasticity, high thermal conductivity, low coefficient of thermal expansion, high adsorption of gases and good chemical stability at high temperatures.

2.1.2 Introduction to Carbon Nanotubes (CNTs)

Carbon nanotubes (CNT) are composed of single or multiple graphene sheets rolled-up to form hollow tubes which are arranged in a concentric manner. CNTs are generally categorized as: 1) Single-Walled Nanotubes (SWNT) and 2) Multi-Walled Nanotubes(MWNT). Figure 2.2 depicts a single graphene sheet rolled up to form a SWNT and a MWNT formed by a concentric arrangement of multiple SWNTs.

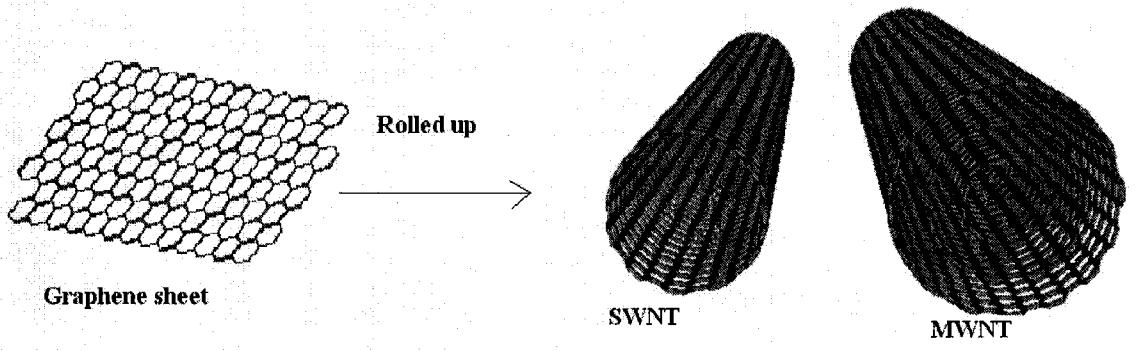

Figure2.2: A schematic of a graphene sheet being rolled up to form a SWNT and a MWNT

The ends of these hollow tubes can be open or closed. The latter case is observed when a fullerene-like molecule cap is attached on the end of the tube. CNTs were first discovered by Iijima [1] while observing the cathode deposits produced by the graphite arc discharge using HRTEM. The carbon atoms in the CNT structure are assembled in

pentagonal or hexagonal rings, thus both sp^2 and sp^3 hybridization is observed in CNTs. The diameters of CNTs are in the range of 1nm to 50 nm where as their length can achieve from a few microns to millimetre ranges. Due to the high length to diameter ratio (i.e. aspect ratio), CNTs can be classified as quasi one dimensional (1-D) materials.

2.1.3 Atomic Structure of CNTs

CNTs are formed by rolling up of graphene sheets with different diameters and angles of twist. The atomic structure of the CNTs is defined by three parameters: the radius (r), the length of the cylinder (l), and the angle of chirality (θ). The angle of chirality is the angle between the chiral vector C_h and the nearest zigzag of carbon-carbon bonds [2]. As it can be observed from Figure 2.3, chiral vector C_h connects to sites for the roll-up of the graphene sheet. The magnitude of this vector is calculated by the equation below and is equal to the circumference of the CNT.

$$C_h = n\vec{a}_1 + m\vec{a}_2 \qquad (1)$$

Where the vectors $\vec{a}_1$ and $\vec{a}_2$ are the graphene lattice unit vectors, and the two intigers (n,m) representing the indices of carbon atoms in the lattice [3].

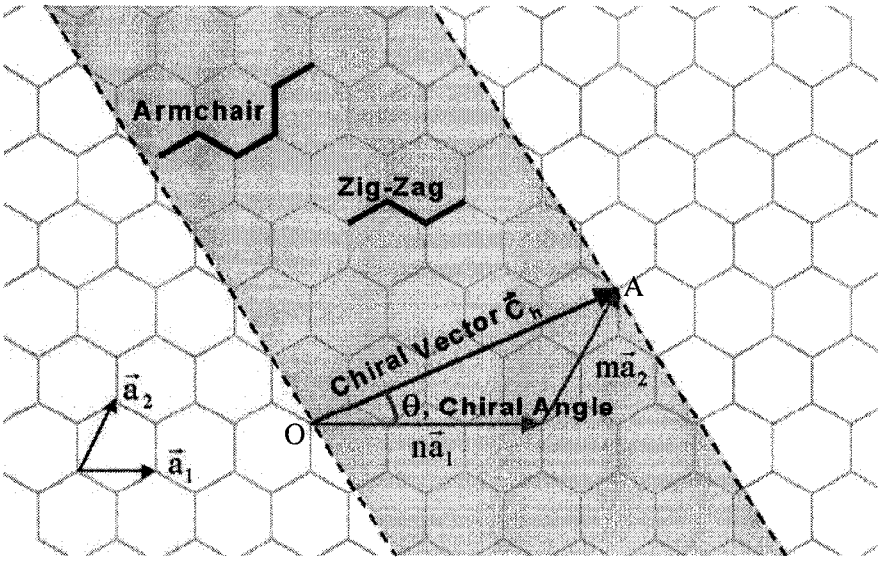

Figure 2.3: Angle of chirality, θ and the chirality vector C_h on a graphene sheet [3].

The chiral angle for all tubes varies between 0^{o} and 30^{o}. Rolling up the graphene sheet along one of the two symmetry axis gives an achiral tube. An achiral tube is a tube with mirror symmetry and is formed when the chiral angle is equal to 0^{o} or to 30^{o} [2]. When $\theta = 30^{o}$, the tube is called as an 'armchair' nanotube. The chiral vector of an armchair tube is (n,n). When $\theta = 0^{o}$, the tube is defined as a 'zigzag' nanotube. The chiral vector of a zigzag tube is (n,0). Rolling up the graphene sheet in a direction different from the symmetry axis gives a chiral tube in which the equivalent atoms of each unit cell on the tube are aligned on a spiral. When θ is between 0^{o} and 30^{o}, a chiral tube is formed [4]. The carbon bonds arrangement of the armchair and the zigzag CNTs are indicated by arrows in Figure 2.3. Achiral and chiral tubes are shown in Figure 2.4.

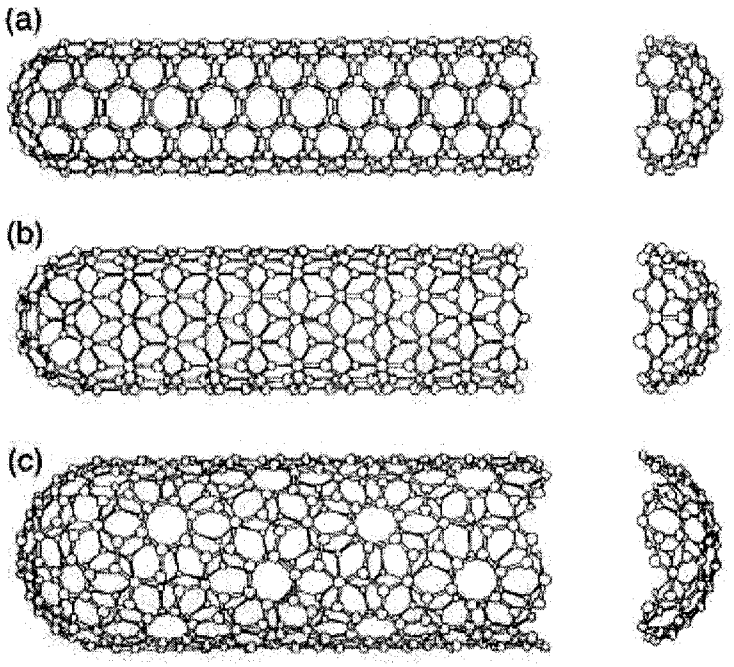

Figure 2.4: Examples for (a) armchair (n,n) where $\theta=30^{o}$ (b) zigzag (n,0) where $\theta=0^{o}$ and (c) chiral tubes where $0^{o} < |\theta| < 30^{o}$ (c) [2].

2.2 Properties of CNTs

After the discovery of CNTs, research groups interested in CNT production focused on determining the physical and chemical properties of these new materials. They conducted research in determining the mechanical, electronic, thermal and chemical characteristics of their product. This section introduces some of these exceptional properties investigated by these research groups.

2.2.1 Mechanical Properties of CNTs

CNTs are known to be very strong materials. It has been demonstrated that they possess both high Young's modulus of elasticity and tensile strength. There have been reports that the CNTs are 10 to100 times stronger than steel while being six times lighter [2, 3]. The stiffness and axial strength observed with CNTs are attributed to the available carbon-carbon sp^2 bonds [2]. Typical carbon fibers are reported to show values of 680 Gpa for Young's modulus. Average values of 1.8 TPa and 1.25 TPa are reported for MWNTs and SWNTs, respectively [3]. The tensile strength associated to CNTs was predicted to be in the range of 13 to 52 GPa by a model developed by Yu *et al* [5]. Also direct tensile strength measurement method developed [6] yielded values ranging from 11 to 63 Gpa, which is in accordance with the values obtained by the model. As a result of their excellent elastic and tensile strengths, CNTs can be used as reinforcing agents for a variety of materials.

2.2.2 Electronic properties of CNTs

The chiral vector defined previously in the atomic structure of CNTs, determine the electronic properties of CNTs. CNTs can show either metallic or semiconducting properties depending on the tubes' diameter and chirality [7]. If $2n + m = 3p$ where p is an integer then the CNT is metallic, otherwise semiconducting [8]. Therefore all armchair CNTs (n,n) and one third of zigzag and chiral CNTs are metallic [9]. It is important to

note that each concentric graphene sheet in MWNT has individual electronic properties, but even if one acts as a metal the whole CNT will act as a metal. The metallic properties of CNTs allow them to carry large current densities and have low electrical resistivities. The semiconducting properties permit CNTs to be used as semiconductors without requiring any doping.

2.2.3 Field Emission Properties of CNTs

Field emission is related to the emission of electrons from the surface by imposed electric fields. The emitted current depends directly on the local electric field, E_s, at the emitting surface and on the surface work function, Φ [10]. The CNTs provide numerous properties for applications requiring field emission properties. CNTs are shown to emit electrons at low voltages due to their unique geometry. The fact that CNTs have sharp tips and extremely large aspect ratios favours a strong local electric field concentration, providing a mechanism for good electron emission [11]. There seems to be a growing demand for CNTs as electron field emitters because of their high electrical conductivity, high mechanical stiffness, chemical stability, and capability to carry high current density. This property of CNTs will make them find applications in areas where electron sources are extensively used such as cathode tube rays, flat panels and electron beam instruments[9].

2.2.4 Thermal Properties of CNTs

CNTs are extremely good heat conductors. The thermal conductivity values of MWNT and SWNT are around 3000 W/K m [12] and 6600 W/K m, respectively [13]. When compared to the thermal conductivities of copper and aluminum, the reported values are an order of magnitude higher. This property of CNTs is promising in order to produce heat transfer composites and fluids. It is was demonstrated by Biercuk *et al* [14] that with a 1 wt.% of MWNT in MWNT/epoxy composite, an increase up to 125 % in thermal conductivity is achieved.

2.3 Synthesis Methods of CNTs

The general production recipe for CNTs is similar for all the production methods mentioned in literature. CNTs are grown from metal nanoparticles deposited (or formed) on desired substrate surface at a specific temperature range. The available carbon for CNT growth is achieved by initial atomization of a carbon containing raw material. Metal nanoparticles serve to avoid closing of early-formed carbon molecules and thus facilitate growth of CNT. The synthesis methods for CNTs can be divided into three: 1) vaporization of metallically doped graphite (i.e arc dischare and laser ablation) 2) catalytic pyrolysis of hydrocarbons (i.e chemical vapour deposition) and 3) dissociation of carbon by thermal plasma torch. Among the methods mentioned above pyrolysis methods can be easily scaled-up to industrial scales and are less expensive than arc discharge and laser ablation methods. Descriptions of arc discharge, laser ablation and pyrolysis methods will be given in this section. Observations and findings of researchers employing CVD processes will be given in detail.

2.3.1 Arc Discharge

This method involves the constructing of an electric arc (AC or DC) between two cylindrical graphite electrodes in a helium atmosphere. Metal catalysts are introduced by doping the cylindrical graphite electrodes with metal powders. The discovery of CNTs was achieved with this method by Iijima [1]. Since then the method is developed to produce CNTs with desired structures (MWNT or SWNT).

The applied voltage and current for this method are in the ranges of 20 – 25 V and 50 - 120 A, respectively. The arc is ignited by touching the electrodes together and then separating them immediately. The arc discharge serves to vaporize the metallic powder which acts as a gas phase catalyst. The graphite anode surface is vaporized due to large heat flux from the arc and serves as the source of carbon available for CNT growth. The deposition of carbon nanotubes is observed on the cathode. Along with CNTs a large quantity of carbon soot condenses on the walls of the reactor. Figure 2.5 is a schematic of the setup used for this method.

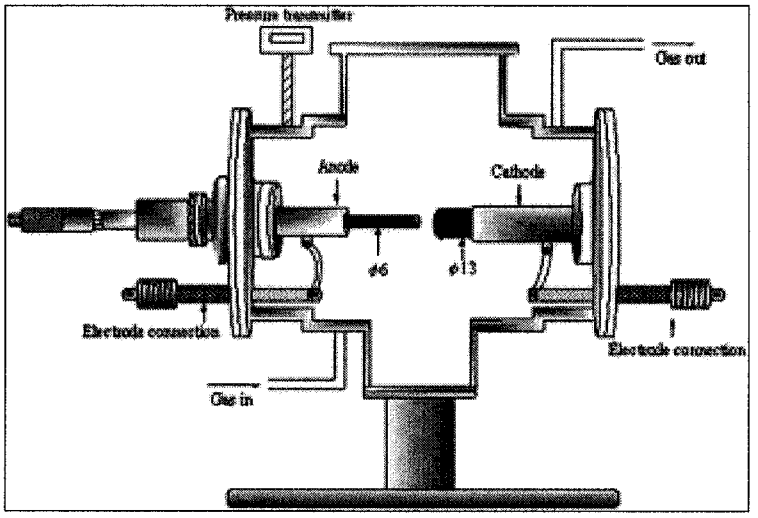

Figure2.5 Schematic of a setup used for an electric arc discharge method to synthesize carbon nanotubes [28]

Even though this method produces high purity CNT at the lab scale the possibility for scale-up of this process is low. It has been shown previously that a power increase of the arc device decreases the CNT production and eventually eliminates all CNT produced.

2.3.2 Laser Ablation

In this method, vaporization of a graphite solid doped with metal catalysts is achieved by laser ablation. The solid target is placed in a tubular quartz furnace which is heated up to a temperature in range of 800 – 1500 C. A Nd:YAG laser is focused on the target. The vaporized carbon structures are carried from the target by a flow of argon gas to a water-cooled copper collector found at the exit of the reactor, where the carbon structures are deposited. The pressure inside the tube is controlled by a vacuum pump at around 0.70 atm. The pioneers in this method, Guo *et al* [15] showed that they were able to convert 50 % of the vaporized carbon to SWNT by using a mixture of nickel and cobalt as a catalyst with a minimal amount of amorphous carbon content. Figure 2.6 is a schematic of the setup they have employed.

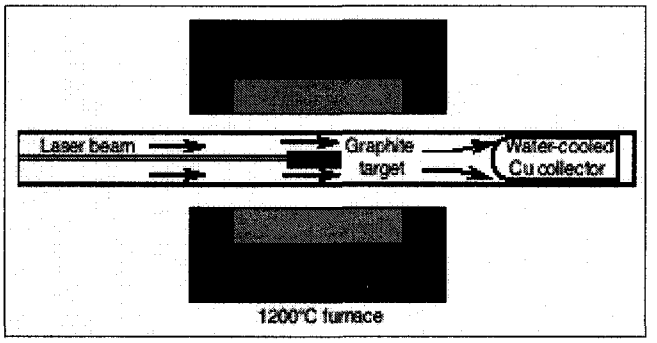

Figure 2.6. Schematic of the laser ablation setup used by Guo *et al* at Rice University [15]

2.3.3 Catalytic Pyrolysis of Hydrocarbons

In this method CNT synthesis is achieved via pyrolysis of a mixture of hydrocarbon and catalyst at high temperatures in an inert atmosphere. An organometallic compound dissolved in a liquid hydrocarbon serves as the catalyst and carbon source, respectively. For example, the method developed by Andrews *et al* [16] employs ferrocene ($C_{10}H_{10}Fe$) dissolved in xylene as the catalyst/carbon source mixture. The reactor consists of a two stage tubular quartz reactor at atmospheric pressure as seen in Figure 2.7. The catalyst/carbon source mixture is introduced in liquid form and is vaporized in the first stage of the reactor (pre-heater), and then the vaporized mixture is carried into the furnace by carrier gas (argon). The temperature of the second zone is set at a value between 650 and 1050 °C. At this temperature the catalyst precursor decomposes to form metal nanoparticles to initiate CNT growth in the gas phase. Finally the soot containing CNT is collected from the inner walls of the quartz tube and water cooled copper collector found at the exit of the reactor.

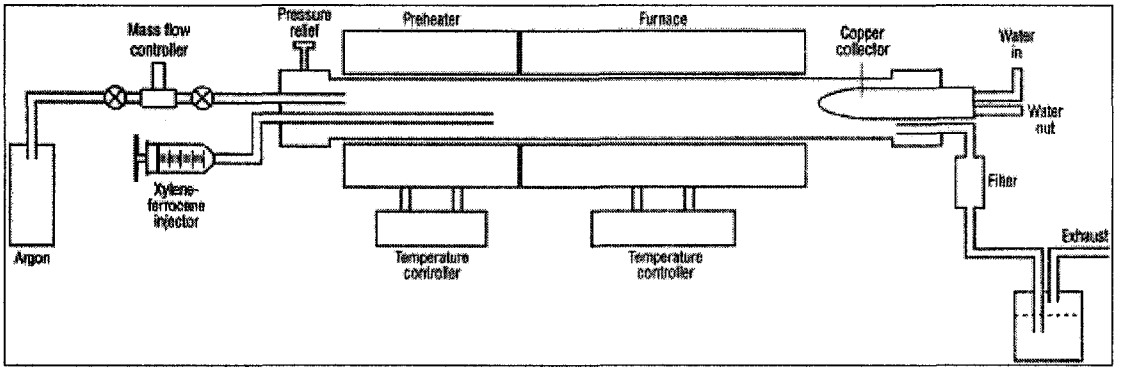

Figure 2.7 The schematic of the catalytic pyrolysis method employed by Andrews *et al* [16]

2.3.4 Chemical Vapour Deposition

The CVD process involves growing CNT on a temperature controlled substrate (between 600 and 1000°C) trough the decomposition of a carbon-containing gas. There are two commonly used CVD methods to decompose a carbon-containing gas to generate the carbon precursors for CNT synthesis: 1) Thermal CVD [17, 18] and 2) Plasma Enhanced (PE) CVD [19, 20]. To catalyze the formation of CNT, metallic nanoparticles of transition metals such as nickel, cobalt and iron are deposited onto the surface of the substrate desired for CNT growth. The carbon atoms, generated from the decomposition of the carbon-containing gas, dissolve and saturate the metal. Precipitation of carbon from the metal catalyst particles leads to the growth of CNT on the surface of the substrate. The schematics of the two types of CVD are given in Figure 2.8.

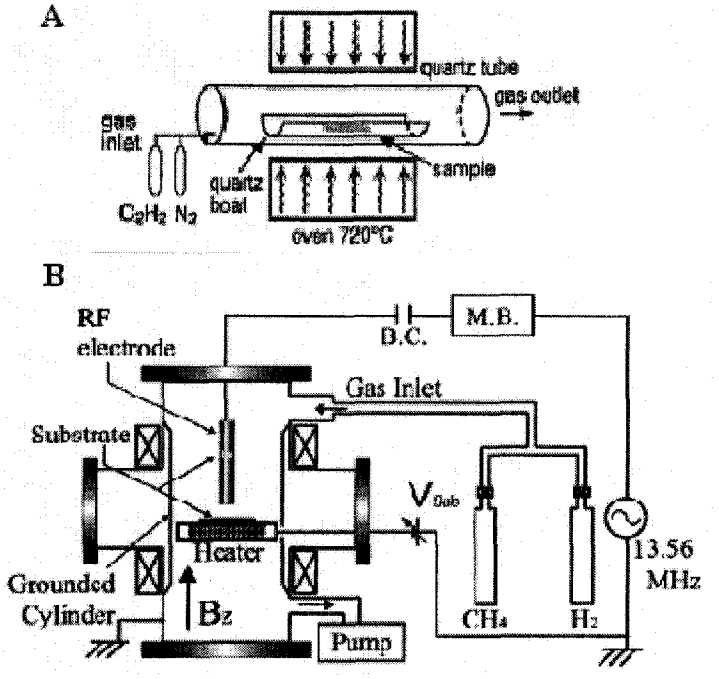

Figure 2.8 Schematics of the setups used for A) thermal CVD [21] and B)PE-CVD [22]

The thermal CVD reactor is a simple design which consists of a quartz tube placed inside a tubular furnace (Figure 2.8 A). The substrates to grow CNTs are placed in the center of the reactor and the carbon-containing gas along with a inert carrier gas is introduced into the system. The inert gas is required to purge the system off of air so that

the substrates are not oxidized when the furnace is being heated. The decomposition of carbon precursor gas occurs at a desired temperature between 600 and 1000°C. The temperature and the size of catalyst nanoparticles determine the shape and purity of CNTs produced.

The PE-CVD systems involve the decomposition of a carbon containing gas trough the creation of a plasma. Plasma is created by a variety of sources including microwave [19] and radio frequency (RF) (Figure 2.8 B) between the two electrodes in a low pressure atmosphere. The advantages of this type of setup include; ability to grow CNTs at low synthesis temperatures as well as possibility of vertical growth and alignment of CNTs.

The effect of carrier gas on the CNT production rate and purity was investigated by Zhao *et al* [23]. A granulated metallic catalyst of Ni:Cu:Al = 2:1:1 was placed in the CVD reactor operating at a synthesis temperature of 750 °C. They used methane (CH_4) as the precursor gas. They kept the CH_4 flowrate constanst and investigated three cases of production when 1) no carrier gas present 2) only H_2 present and 3)only N_2 present. In case 1, the sample produced contained high amounts of amorphous carbon and in case 2 even though clean CNTs were produced the rate of production was minimal. They attributed the lack of amorphous carbon present in this case to the combination of amorphous carbon with H_2 more readily then CNT with H_2. However case 3 showed promising CNT production quality and rate, suggesting that nitrogen is a good carrier gas. It is important to note in this case that with careful combination of the right concentrations of gases it is also possible to reduce both the amorphous carbon content as well as maintaining high production rates.

By the works of Lee *et al* [24] it was demonstrated that deposition of nickel and cobalt as a film over a silicon oxide surface provided good catalytic activity for CNT growth. They used wet hydrogen fluoride and ammonia gas etchings as pretreatment methods. Their precursor and carrier gasses were acetylene (C_2H_2) and Argon (Ar), respectively. The synthesis temperature was chosen to be 950°C. It was pointed out in

this work that ammonia etching was necessary to obtain high density of nucleation sites. According to their work, ammonia pretreatment causes etching of the surface of the catalytic metal which results in catalytic metal particles acting as nucleation seeds. The size of the CNT diameter is related to the size of the metal particle. They have achieved to produce carpets of vertically aligned CNTs at large areas of their substrates.

Various other research groups worked on the enhancement of CNT production by deposition of various catalyst particles and films on silicon [25] and on graphite substrates [26]. On the other hand, the growth of CNT directly onto metal or metal alloy surfaces might be useful in some applications such as electrochemical double layer capacitors (EDLC) or reduction of arc erosion for electrodes used in plasma torches.

Park *et al* [27] investigated the effect of HF and H_2 plasma pretreatment of stainless steel surfaces to be used as EDLCs. They employed a rf powered PE-CVD setup. Their precursor gas was acetylene (C_2H_2). The syntheses of CNTs were carried at temperatures between 600 and 850 °C. The concentrations and dipping times for HF treatment and flowrate of H_2 were varied. For the substrates that were pretreated with H_2 plasma no CNT synthesis was observed. They concluded that it was necessary to etch the surface with HF prior to CVD in order to produce a dense layer of CNTs. An interesting observation from their work was that, when the surface of the treated stainless steel was examined for elemental composition, HF treated surfaces showed a deficiency of iron (Fe). They could not conclude if this was the reason behind enhanced CNT growth. Their research underlined the link between catalyst particle size and CNT diameter, by showing that increasing the H_2 plasma treatment time following the HF etching, caused the grain sizes of the particles to increase resulting in CNTs with larger diameters.

2.4 Mechanism of CNT Growth

As seen in the previous section, the different synthesis methods show differences in the type of carbon containing raw material, type of metal catalyst and the method of vaporization. Therefore the proposed mechanisms for CNT formation in literature are specific to type of process they employ. In this section only the mechanism for a CVD reactor using a metal catalyst will be studied in detail. Mechanisms of growth associated with other production methods can be found elsewhere [28-30].

Two of the most common mechanisms for CNT formation on metal particles, that have received general acceptance are root and tip growth. Transition metals; iron, nickel and cobalt have been shown to be most effective for CNT production. Combinations of properties associated with these metals are thought to be the reason for enhanced CNT growth. Their properties include: 1) ability to form metastable carbides 2) catalytic activity for decomposition of hydrocarbons 3) allowance for extremely rapid diffusion of carbon trough and over these materials [31].The third property mentioned allows ordered carbon to be produced by a mechanism of diffusion and precipitation.

Synthesis of CNTs on metal surfaces by CVD is generally achieved either by coating a thin film of metal catalysts on semi-conducting (or insulating materials) or by employing directly a solid metal substrate. For, both cases it has been shown by researchers that it is necessary to transform the metal surface into islands of nano-sized catalyst particles. Thus, the diameter of the CNTs synthesized is correlated to the size of the catalyst particles [32]. Figure 2.9 illustrates the root and tip growth mechanisms suggested by Sinnott *et al* in 1999 [31].

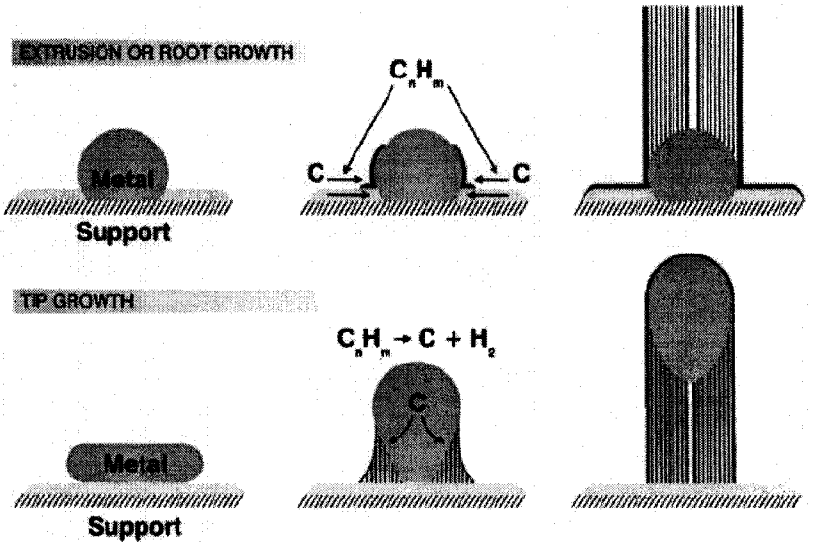

Figure2.9 Mechanisms of carbon nanotube growth as suggested by Sinnot et al A- Root growth B- Tip growth [31]

2.4.1 Root Growth

If the metal particles on the surface of the substrate are spherical as seen in Figure 2.9A, the deposition of carbon atoms occurs on one half of the sphere. The carbon diffuses along the concentration gradient and precipitates on the opposite half. The hollow core specific to CNT formed is attributed to the lack of precipitation trough the apex of the sphere.

2.4.2 Tip Growth

If the metal particles on the surface of the substrate are formed as filaments and have low adherence to the substrate, these particles are detached from the surface by growing CNTs and appear at their tips as outlined in Figure 2.9B. It is possible for the metal particle at the tip of the CNT to further aid growth of carbon nanotubes, thus both tip and root growth mechanisms might be observed.

TEM images of CNTs formed by tip and root growth can be seen in Figure 2.10 a and b, respectively. For Figure 2.10 a the metal nano-particles are found at tips where as in Figure 2.10 b the CNTs grow from these particles and none of those are found on their tips suggesting root growth.

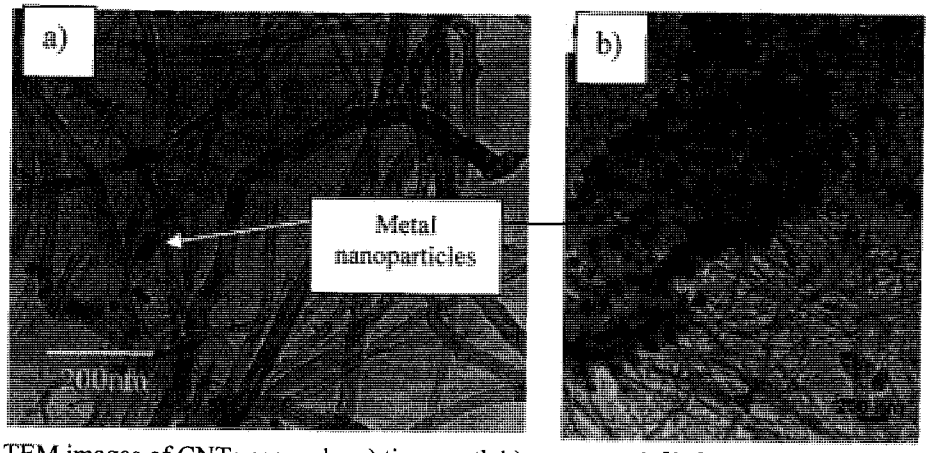

Figure2.10 TEM images of CNTs grown by a) tip growth b) root growth [31]

2.5 Characterization of Carbon Nanotubes

As it was mentioned in previous sections, during the synthesis of CNTs various types of carbonaceous species such as amorphous carbon is present in the product obtained. The physical and electrochemical properties of the produced samples are largely influenced by the content, purity and morphology of the CNTs. For these purposes it is necessary to characterize the samples produced from the CVD process. Morphological characterization of produced samples is achieved by electron microscopy techniques. Researchers have also developed techniques employing Raman spectroscopy and Thermogravimetric Analysis (TGA) to evaluate content and purity of samples. For the purposes of this master's thesis it was also necessary to evaluate surface areas of CNT samples since the electrochemical properties depend highly on the available surface area of the electrode material.

In this section results and observations by researchers in this field along with necessary background information related to physical and electrochemical characterization of CNT samples will be given. Raman spectroscopy and BET surface area methods will be discussed for physical characterization methods. Cyclic voltammetry (CV), method will be introduced for electrochemical characterization purposes.

2.5.1 Physical Characterization

Raman Spectroscopy

Raman spectroscopy relies on the measurement of change in vibrational energy inside a molecule when irradiated with an electromagnetic wave. Most of the photons hitting the molecule will go trough elastic collision but some will either be absorbed or energized by the molecule causing inelastic collisions. These inelastic collisions are responsible for changing the vibration energies in the molecule.

The Raman spectroscopy for CNT samples is achieved by irradiating the sample with an intense source of monochromatic light. The reported values of wavelengths used for analysis of CNT samples are 488, 514, 632 and 785 nm. As the wavelength of the laser used increases a higher signal-to-noise ratio is observed thus a higher resolution. The different species in a given sample will each vibrate at a specific wavelength, therefore Raman spectroscope collects the dispersed light and differentiates it into its wavelength spectrum. Figure 2.11 below shows a typical Raman spectrum of a sample containing carbon nanotubes.

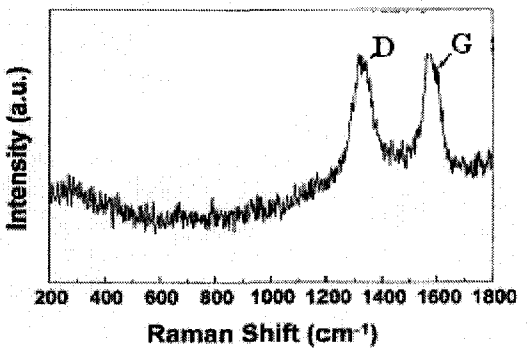

Figure 2.11 Raman spectrum for the vertically aligned CNTs grown on Co deposited SiO_2 substrate, showing the D and G modes[24].

Researchers have observed four types of vibration modes for carbon samples containing CNTs. The disorder mode (D) located in the 1250 cm^{-1} to 1350 cm^{-1} range implies the presence of non-graphitized carbon species such as carbon impurities, amorphous carbon and pentagon rings in the CNT structure. The graphitic mode (G)

located in the 1500 cm^{-1} to 1600 cm^{-1} range results from the graphitic content in the sample. The presence of SWNT and DWNT are characterized by the Radial Breathing Mode (RBM) observed in the 100 cm^{-1} to 350 cm^{-1} range [33].This mode is not observed for MWNT samples. Relatively recently it was reported by Saito *et al* [34] that a fourth mode named G' mode situated in the 2500 cm^{-1} to 2800 cm^{-1} range indicates the long-range order in a sample arising from a two phonon second order scattering process. This process results in the creation of an inelastic phonon that can also be used for characterizing carbon samples containing CNT.

The ratio of intensities of D mode over G mode (I_D/ I_G) is used extensively by researchers to characterize their samples [33, 35]. A low ratio represents a sample with high CNT content. Qian *et al* [33] studied the Raman spectra of mixed samples containing metal impurities, amorphous carbon , SWNT and MWNT. Their research showed that I_D/ I_G remains stable with increasing metal impurities suggesting that metal particles have no effect on the Raman scattering. They have also demonstrated that adding MWNT or amorphous carbon to SWNT samples increases the I_D/ I_G ratio due to the presence of defects in MWNT structure compared to SWNT and non-graphitized content in amorphous carbon. For this reason assessing the purity of MWNT samples using solely I_D/ I_G ratio might provide ambiguous results. For this reason it is suggested by Saito et al [34] and Raffaelle *et al* [36] to employ the G' band peak to determine the quality for a MWNT sample.

Raffaelle *et al* [36] used a constructed sample set of mixtures of MWNTs with carbonaceous by-products at varying concentrations of MWNTs from 0 to 100 %. A 100% MWNT was assigned to the highest purity of sample produced by their CVD setup and by TGA and SEM. They have demonstrated that as the MWNT concentration decreases G' band peak also decreases and finally disappears for 0% MWNT sample (Figure 2.12). The ratios of intensities of D to G (I_D/ I_G) , G' to G ($I_{G'}$ / I_G) and G' to D ($I_{G'}$ / I_D) modes were used to construct calibration curves for MWNT content. They have concluded that for a given range of MWNT concentration $I_{G'}$ / I_D ratio shows largest relative change and thus is more reliable for assessing MWNT quality in CNT samples.

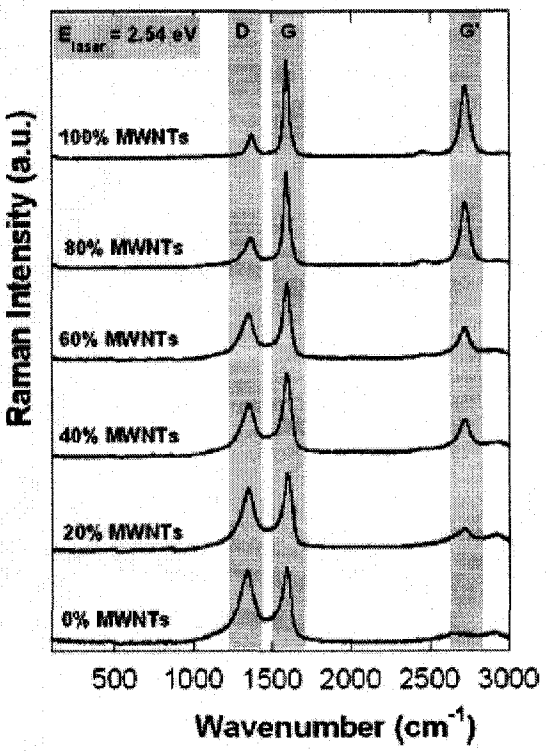

Figure 2.12 Raman spectra showing the decrease in G and G' along with increase in D intensities as the amount of MWNT in the mixture is decreased [36].

The purity of their samples were calculated by solving for X (i.e. purity in % CNTs) in the equation given below:

$$I_{G'} / I_D = 0.31 \exp(0.021X) \qquad (2)$$

Surface area measurement

There are numerous experimental techniques for determination of surface area of porous materials, including small angle x-ray and neutron scattering (SAXS and SANS), mercury porosimetry, electron microscopy, thermoporometry, NMR-methods. Compared to these methods gas adsorption is the most popular one because it allows assesment of a wide range of pore sizes (from 0.35nm upto and greater than 100nm) and is convenient to use and relatively less expensive than other methods mentioned.

The amount of gas adsorbed on a solid surface (W) will depend on the absolute temperature (T), the pressure (P) and the interaction potential (E) between the vapor (adsorbate) and the surface (adsorbent).

$$W = F(P,T,E) \qquad (3)$$

Most of the time the amount of gas adsorbed is measured at constant temperature, therefore the function above reduces to :

$$W = F(P,E) \qquad (4)$$

A plot of W versus P, at constant T, is called the adsorption isotherm of a specific gas-solid interface. The amount of gas desorped from the surface of a material can also be plotted giving us the desorption isotherm. Most of the analytical equipment today relies on the theory that was developed by Bruanuer Emmett and Teller [37] in 1938 to explain the adsortion isotherms of gases. The assumptions and derivations related to this theory can be found in Appendix I.

The most common adsorbtive gas used for determination of surface area is nitrogen (N_2) and helium (He) as the carrier gas. The adsorption occurs at the boiling temperature of N_2 (77 K). Researchers generally use different mixtures of nitrogen (N_2) and helium (He) to vary the pressure of the system, so at different partial pressures of N_2 the amount of N_2 in the gas mixture is detected by thermal detectors and recorded to construct the adsorption isotherm. The shape of the adsorption/desorption isotherms are generally used to evaluate the pore size distribution of the samples.

A single point surface area measurement is the simplest characterization method for surface area analysis of samples. A mixture of N_2 and He at a specific concentration is introduced into the system, where following the adsorption of N_2 , the surface area of the sample is calculated from the amount of N_2 desorped from the sample by the following equation :

$$S_t = V(1 - \frac{P}{P_o})\frac{N_A}{M_V} A_X \qquad (6)$$

Where S_t is the total surface area of the sample, V is the volume of adsorbent (N_2) desorped from the surface, P is the adsorbate pressure , P_o is the saturation pressure of the adsorbate, N_A is Avogadro's number, M_v is the molar volume of a gas at standard conditions (22.414 cm^3/mole) and A_x is the molecular cross-sectional area of an adsorbed nitrogen molecule (approx. 16.2 $Angstroms^2$).

Since the surface area is closely linked to the electrochemical capacitance of electrode materials, values obtained for BET surface areas of CNTs and related observations with regards to capacitance values will be discussed in the next section.

2.5.2 Electrochemical Characterization

Due to the significant demand of carbon based materials as electrode materials for electrochemical capacitor applications, necessary theory and results obtained from researchers involved in this area will be given in this section.

Introduction

Recently, there has been a growing demand for electrode materials to serve as electrochemical capacitors (EC). It has been an important issue to come up with environment friendly electric power sources to reduce pollution caused by combustion engines of automotive systems. Even though conventional battery systems and fuel cells supply high energy they lack the high specific power that would be required for hybrid power sources. As it can be observed from the Ragone plot in Figure 2.13, the ECs can fill the gap between conventional capacitors and batteries. Thus, electrochemical capacitors may improve the performance of batteries in terms of power density, or energy density of the ECs can be improved when coupled with a battery in order to serve as hybrid systems. Additionally, ECs have longer cycle lives than batteries due to negligibly small charge transfer reactions involved.

Principle of energy storage in ECs

Electrical energy in an EC is stored in what is called an electrochemical double layer (i.e. Helmholtz layer) formed at the solid/electrolyte interface. The stored electrical energy depends on the separation of charged species in the double layer. The maximal charge density is observed at the outer Helmholtz plane (i.e. at the centre of the electrostatically attracted solvated ions). Figure 2.14 illustrates this double layer formation.

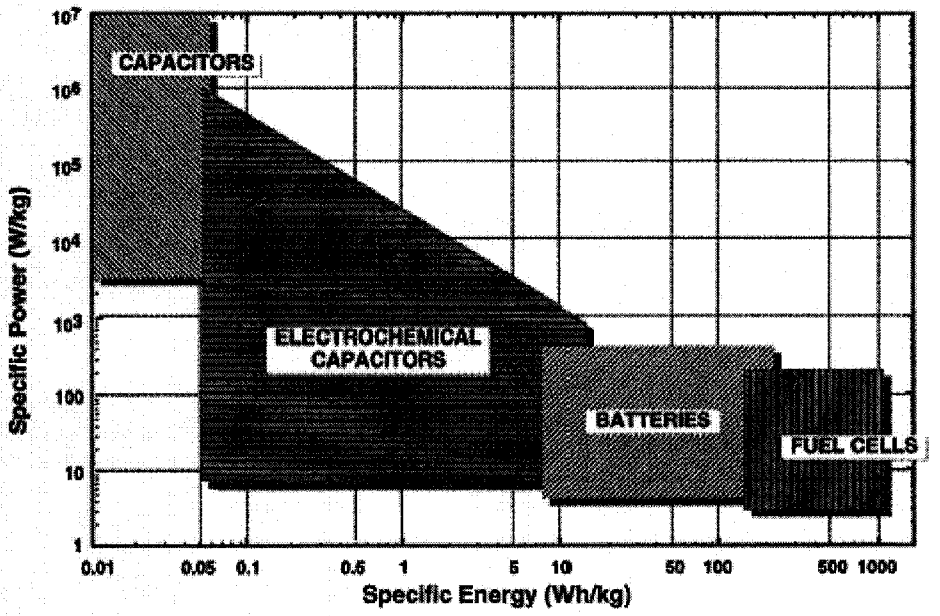

Figure 2.13 Ragone plot showing various energy storage and conversion devices [38]

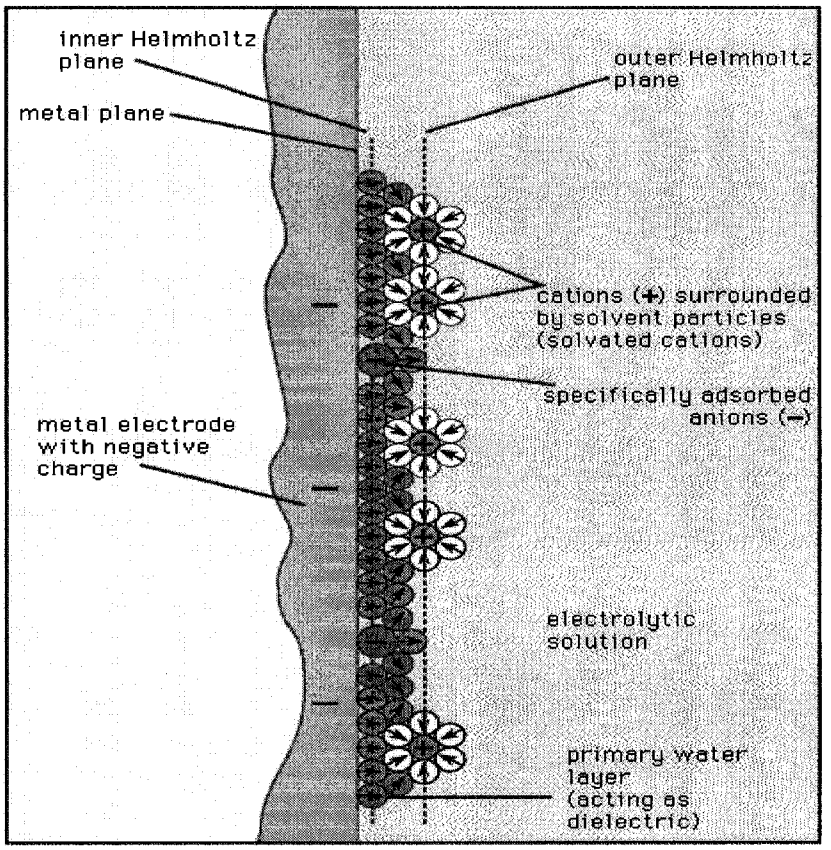

Figure 2.14 Schematic of electrochemical double layer formation on a metal surface [39]

The electrical capacitance stored in the electrochemical double layer is proportional to the surface area of the electrode (S), the relative permittivity of the solution ε, and is inversely proportional to the thickness of the double layer, d [40]:

$$C = \frac{S\varepsilon}{d} \qquad (7)$$

In strong and concentrated electrolyte solutions the double layer has a thickness of a few angstroms [38]. Theoretically, higher the surface area and the concentration of the electrolyte, the higher the value of capacitance should be. However, researchers have demonstrated that the electrochemically active surface area for charged species is quite different from measured surface area of electrode materials by gas adsorption methods. This is due to the fact that micropores available in materials such as carbon are not accessible to solvated ions [39].

Determination of Specific Capacitance

Capacitance of electrode materials is calculated from a variety of electrochemical techniques such as cyclic voltammetry (CV), galvanostatic charge – discharge curves and also impedance spectroscopy. It should be noted that the specific capacitance values reported in the literature are not consistent, generally because of the differences in experimental setup employed. Figure 2.15 a below represents the setup for the three electrode cell used in typical lab cells, and Figure 2.15 b represents the two electrode system which represents a real capacitor device.

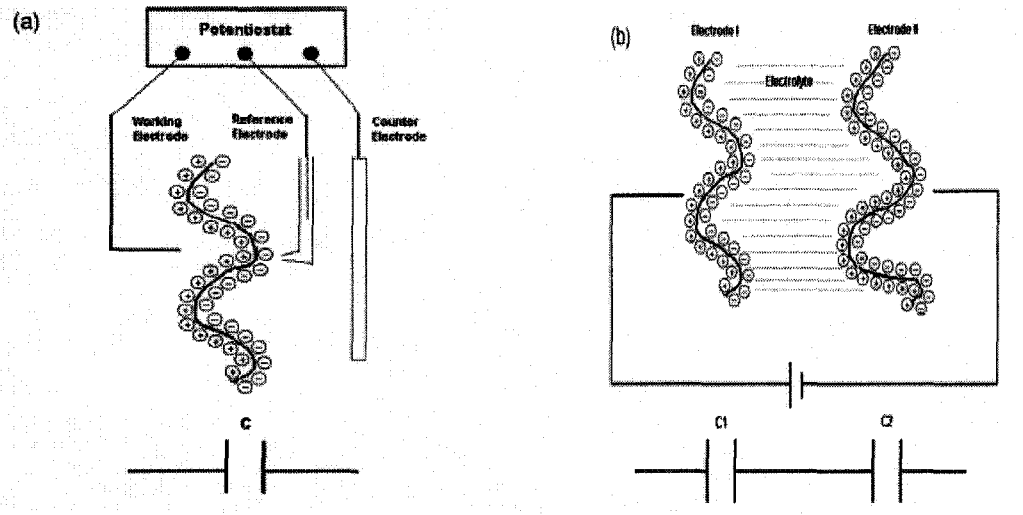

Figure 2.15 Schematic and representative electrical circuit of a) 3 electrode b) 2 electrode systems[40]

Assuming a weight of m for each individual electrode, the capacitance observed will be the same for each individual electrode:

$$C_1 = C_2 = C \quad (8)$$

The capacitance measured for the two electrode system therefore is

$$C_{2E} = \frac{1}{2} C \quad (9)$$

Thus, the specific capacitance for this system is

$$C_{spec\text{-}2E} = C_{2E} / 2m = C/ 4m \quad (10)$$

However for the three electrode system, the double layer capacitance is simply

$$C_{3E} = C \quad (11)$$

and consequently,

$$C_{spec\text{-}3E} = C/m \quad (12)$$

Finally the relationship between a two electrode and three electrode configuration is

$$C_{spec\text{-}3E} = 4\, C_{spec\text{-}2E} \quad (13)$$

Pseudocapacitance

Supercapacitors combine two kinds of energy storage, an electrostatic attraction as in electrochemical double layer capacitance and faradaic reactions similar to processes observed in batteries. Pseudocapacitance occurs when the charge q is a continuously changing function of potential, E. The term "pseudo" refers to the fact that the capacitance is enhanced trough quick faradaic charge transfer reactions and not only from

electrostatic charging. The deviation from ideal electrochemical double layer capacitor behaviour due to pseudocapacitance will be illustrated in the next section.

Cyclic Voltammetry (CV)

Cyclic voltammetry is a kind of potentiodynamic electrochemical measurement. In other words, the applied electrode potential follows a cycling ramp (linearly increasing and decreasing) potential against time curve as in Figure 2.16.

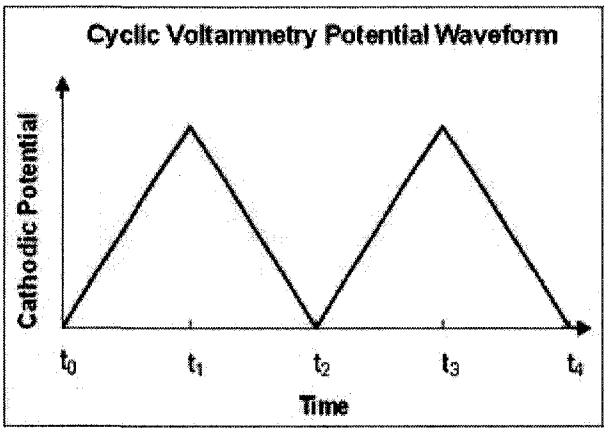

Figure 2.16 Curve illustrating the cyclic behaviour of potential in CV with respect to time

The potential is measured between the reference electrode and the working electrode, whereas the current is measured between the working electrode and the counter electrode. The data obtained is plotted as current (I) against potential (V). Figure 2.17 illustrates the CV curve for an ideal double layer capacitor as well as a CV curve obtained for a carbon electrode showing pseudocapacitance.

For an ideal double layer capacitor material the CV reveals a rectangular shape. In this type of energy storage, purely electrostatic attractions plays a role, therefore the current is independent on the potential. Upon reversal of the potential scan, the sign of the current is inverted immediately. However for materials showing pseudocapacitive behaviour, deviation from a rectangular shape is observed and a delay of potential is remarkable during reversing of the potential scan.

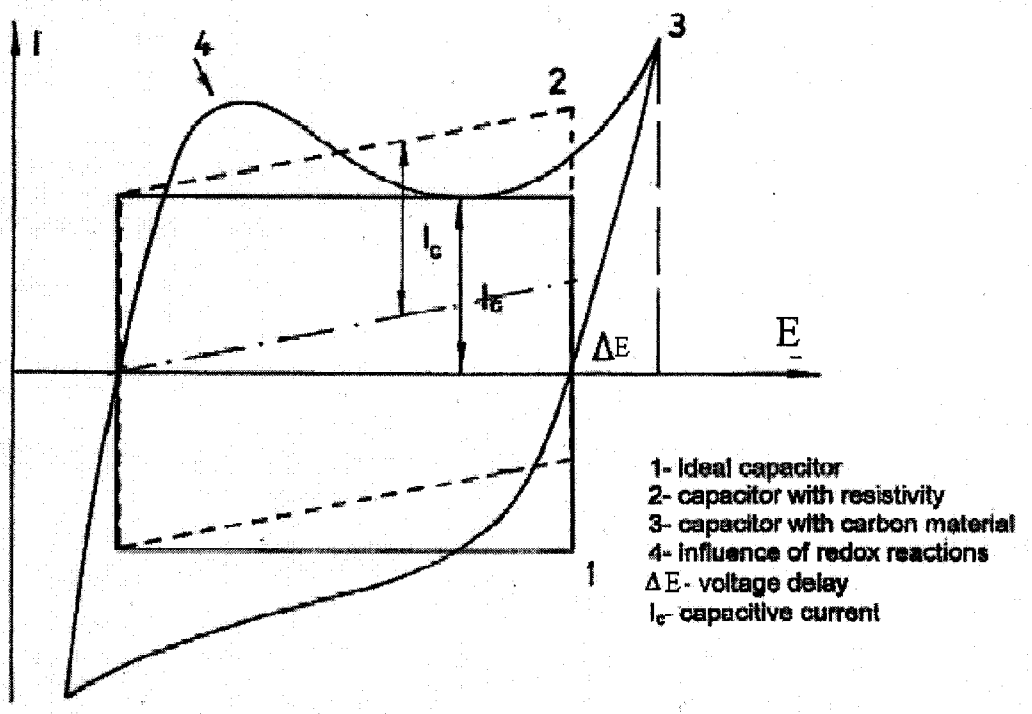

Figure 2.17 Comparison of typical cyclovoltammogram for an ideal electrochemical capacitor and a capacitor showing pseudocapacitive behavior [39]

By performing a CV measurement on the CNT electrodes prepared, information on: the potential range in which the cell needs to be operated, existence of pseudocapacitive behavior, power characteristics and an average current for carrying galvanostatic charge/discharge analysis can be obtained.

Capacitance is related to the current by the following equation:

$$I = C \times \frac{dE}{dt} \qquad (14)$$

where *dE/dt,* is the rate of change of potential with respect to time, it is also referred as scan rate, *v*. Thus for an ideal electrochemical capacitor the slope of the plot of capacitive current, I_c against scan rate, *v* will give the capacitance of the material, C. Specific capacitance, C_{spec} is calculated by dividing this value by the mass of material.

Energy density of the electrode at a chosen potential can be calculated by the following equation:

$$E = (½)\, C_{spec}\, E^2 \qquad (15)$$

Carbon materials in ECs

From the available carbon materials, the most attractive from an economical point of view are the activated carbons for the building of electrodes. Studying different types of activated carbons, Shi *et al* [40, 42] demonstrated that there is an absence of proportionality between the specific capacitance and surface area They concluded that the accessibility of the ions in the electrolyte into the micropores (< 2nm) is an important factor. Since most of the activated carbons consist largely of micropores electrochemical accessibility of ions is hindered. Additionally, the microporous texture also determines the ionic conductivity of ions inside the pores. Their work concluded that, higher the surface area, smaller the pore size and lower is the conductivity. From a practical point of view, it is pointed out that carbons with large percentage of meso (2 -50 nm) or macropores (> 50nm) are found to be more convenient as capacitor electrodes for high power super capacitors (SCs). Such capacitors can deliver high energy at high rate, although they can store less total energy. Table 2.1 below shows the capacitance and specific surface area of a variety of activated carbons (obtained from Spectracorp).

Table 2.1 Comparison of specific capacities and surface areas of activated carbons [40]

Carbon	Specific capacity (F/g)	BET surface area (m^2/g)
M-10	55.95	1370
M-14	57.20	1223
M-15A	78.10	1800
M-15B	55.80	1624
M-15C	63.34	1518
M-20	100.00	2130
M-30	62.90	2571
A-10	35.30	1150
A-20	41.20	2012
SACF-20	48.80	1839
SACF-25	27.90	2371

More recently, the use of carbon nanotubes (CNTs) in the building of capacitor electrodes has emerged as an alternative material to possibly replace activated carbons. Different ways of production methods will yield CNTs with slightly different morphologies. Generally the advantages of using CNTs involve very high conductivity

(thermal and electrical along the tube length), chemical and mechanical stability as well as unique mesoporous morphology.

In 2000, Frackowiak and Beguin *et al* [43] investigated using differently grown MWNTs in capacitor applications. Morphological characterization of MWNTs was achieved via transmission electron microscopy. Braunerr- Emmett- Teller (BET) surface area and mesopore volume was obtained through Nitrogen adsorption/desorption isotherms at 77 K. MWNTs with open ends were produced by catalytic decomposition of acetylene on silica at 700 °C using cobalt supported on silica(CNT#1). A fishbone morphology (resembling nanofilaments) was obtained when this previous procedure was applied at 900 °C (CNT#2). The silica and cobalt particles were removed by hydrofluoric and nitric acids. When MWNTs were produced from decomposition of acetylene at 600 °C using NaY zeolite as a support for cobalt particles, graphitic type layers parallel to the tube axis with closed tips were observed(CNT#3). Chemical vapor deposition (CVD) of propylene at 800 °C within the pores of an Alumina template resulted in straight and rigid nanotubes of large diameter (CNT#4). Carbon electrodes were prepared as pellets by pressing a mixture of 85wt% of MWNTs with 5wt% of acetylene black and the remaining is PVDF binder.

Capacitative properties of the nanotubes are evaluated using the electrochemical data obtained from cyclic voltammetry, galvanostatic discharge and electrochemical impedance spectroscopy for a two electrode Swagelok type cell with 6 mol/L KOH as the electrolyte (refer to Table 2.2). The highest specific capacitance of 80 F/g was observed for MWNTs obtained by catalytic decomposition on cobalt supported silica at 700 °C (CNT#1). This type of MWNT had the highest surface area and mesoporous volume. There seemed to be a good correlation between surface area and specific capacitance but CVD grown MWNTs had moderate specific capacitance although the values of surface area and mesoporous volume were relatively high. This situation is attributed to the hydrophobic character of the CVD grown MWNTs suggested by the small value of oxygen content when compared to the others. It is concluded that oxidation of MWNTs enhances capacitance both through possible pseudofaradaic reactions and increased

hydrophilicity, thus enabling better wetting of the electrode material (i.e. better electrode/electrolyte contact).

Table 2.2 Specific capacity, BET specific surface, mesopore volume and percentage of oxgen of CNTs [16]

MWNTs	Specific capacity (F/g)	BET surface area (m^2/g)	Mesopore volume (cm^3 STP/g)	O_2 (wt %)
CNT#1	80	411	435	10.8
CNT#2	62	396	381	4.6
CNT#3	4	128	269	0.8
CNT#4	36	311	643	<0.3

Enhancement of capacitance through pseudofaradaic reactions

The enhancement of specific capacitance for carbon materials through pseudofaradaic reactions is possible through : 1) chemical activation of carbon materials for increased surface functionality, 2) formation of carbon and electrically conducting polymer (ECP) composites, 3) insertion of electroactive particles of transition metals oxides (e.g. RuO_2, TiO_2 ...).

Chemical Activation of carbon nanotubes

It is a known fact that oxidative treatment enhances specific capacitance of electrodes based on carbon materials. It is largely attributed to the fact that surface functionalization induces pseudofaradaic reactions.

In 1997, Niu *et al* 's work [44] on electrochemical capacitors from CNTs revealed that nitric acid treatment of purchased nanotubes increased their surface area from 250 m^2/g to 430 m^2/g. The functional groups introduced on the surface carbons involved: -COOH, -OH and >C=O. The CNTs were obtained from Hyperion Catalysis International (Graphite Fibrils^{TM}). The specific capacitance measured for a cell, consisting of two CNT

electrodes separated by a polymer separator (Celgrad) and 38 wt% H_2SO_4 as the electrolyte, was 104 F/g.

Additionally in previously mentioned work of Frackowiak *et al* in 2000 [43], treating MWNTs obtained by decomposition of acetylene at 700 °C in 69 % nitric acid solution at 80 °C for 1 hour resulted in increase of specific capacitance from 80 F/g to 137 F/g. For these treated MWNTs only a moderate increase in surface area was observed (from 410 to 475 m^2/g). Impedance spectroscopy measurements for these treated CNTs revealed that there is a high resistance of charge transfer, so a significant increase in capacitance has limited practical application. This resistance is associated with the way the electrodes were prepared. The CNT electrodes were prepared as pellets containing a mixture of CNT powder, acetylene black and PVDF. The pellets were connected to the electrochemical cell trough inserted metal current collectors. This reduced contact between the active CNT electrode and the metal current collectors resulted in the increased resistance. This could be overcome by growing CNTs directly on metal current collectors to reduce this contact resistance.

Activation of CNTs through KOH treatment is also reported by Frackowiak *et al* in 2002 [45]. MWNTs prepared by 1) decomposition of acetylene at 700 °C on cobalt supported silica (CNT#1) 2) decomposition of acetylene at 600 °C on Co particles from a solid solution of cobalt oxide and magnesium oxide (CNT#5) were selected for chemical activation. It was observed that specific surface area of MWNTs was increased significantly after KOH activation from 430 to 1035 m^2/g and from 220 to 885 m^2/g for the two types of MWNTs, respectively. The characterization by N_2 adsorption / desorption at 77 K, revealed development of micropores in the activated samples. It is underlined that the capacitor performance is strongly dependant on both types of pores. For efficient charging of the electric double layer, a developed surface area is required and the presence of micropores is crucial. The main role of the mesopores is the transport of solvated ions from the electrolytic solution to the electroactive surface. Therefore, the value of the capacitance is controlled by micropores, but it is the presence of mesopores that allow the capacitors for high power operations. The specific capacitance of the two

types of MWNTs measured in an acidic medium (1 M H_2SO_4) were 95 F/g and 85 F/g, respectively. Table 2.3 summarizes the effects of treatments on CNT electrodes prepared by different methods.

Table2.3 Oxidative treatment to various CNTs and observed changes in specific surface area and specific capacitiy

Treatment	Change in Specific capacity (F/g)	Change in BET surface area (m^2/g)
Nitric acid treatment to Hyperion Graphite Fibrils	78 to 104	250 to 430
Nitric acid treatment to CNT#1	80 to 137	410 to 475
KOH treatment to CNT#1	80 to 95	430 to 1035
KOH treatment to CNT#5	15 to 85	220 to 885

Carbon nanotube/conducting polymer composites

One big advantage of using the ECP/CNTs composite materials is the possibility of building electrodes without any polymeric binder, while keeping sufficiently good mechanical properties.

In 2001, again Frackowiak and Beguin *et al* [46] demonstrated that depositing electrically conducting polymer (ECP), polypyrole (PPy), on commercially available MWNTs (Hyperion Graphite Fibrils^{TM}) increased the capacitance significantly. Employing the same assembly of the capacitor as in their previously mentioned work, but this time using 1 mol/L H_2SO_4 as the electrolyte, they have achieved a value of capacitance of 172 F/g. Compared to pure Hyperion Graphite Fibrils (78 F/g) and to pure PPy (ca. 90 F/g), there is a considerable enhancement in capacitance trough association of these two materials. It is also mentioned, that enhancement of capacitance comes with a limited durability, due to poor stability of PPy during cycling.

Recently, in 2005 Frackowiak and Beguin *et al* [47] published a paper on supercapacitors based on conducting polymers/nanotubes composites. Their recent research involved testing two additional CNT/conducting polymer composites of polyaniline(PANI) and poly-(3,4-ethylenedioxythiophene) (PEDOT) as supercapacitor

electrode materials. The MWNTs were synthesized by acetylene decomposition on a CoxMg(1-x)O solid solution precursor of catalyst at 600 °C.

The PANI composites were prepared by immersion of MWNTs into an aqeous solution of the monomer and by addition of an oxidant such as $FeCl_3$, $Fe(ClO_4)_3$ or $K_2Cr_2O_7$. Whereas the polymerization of PEDOT was carried in aprotic medium such as acetonitrile, since PEDOT monomer has limited solubility in aqueous medium. All the composites were prepared to contain 20 wt.% MWNTs and 80wt% ECP. Again cycling voltammetry, galvanostatic charge/discharge and impedance spectroscopy were used to analyze electrochemical properties of the composites and it was proved that 20wt% MWNTs is sufficient to ensure a good permeability for the electrolyte. The specific capacitances of Ppy/CNT, PANI/CNT and PEDOT/CNT composites employed in a two electrode cell with 1 mol/L H_2SO_4 were 200F/g, 360 F/g and 100 F/g, respectively. Although PEDOT/CNT composite showed the lower specific capacity, it showed perfect stability during cycling. PANI/CNT composite loses 10% of its initial discharge capacitance in 100 cycles, but maintains a steady value thereafter. Table 2.4 below compares the specific capacitances of mentioned ECP/CNT composites.

Table 2.4 Comparison of specific capacities of various ECP/CNT composites

ECP/CNT composites	Specific capacity (F/g)
Pure Ppy	90
Hyperion Graphite Fibrils/Ppy	172
CNT#5/Ppy	200
CNT#5/PANI	360
CNT#5/PEDOT	100

Carbon nanotubes functionalized with metal oxides

Although ECP/CNTs showed good specific capacitance, the demand for high cycle life (>100,000) has led to other alternatives. Transition metal oxides attached on MWNTs are expected to have enhanced stability as well as good electrochemical properties. RuO_2 is well known as an electrode material showing high performance for electrochemical capacitor because of its multiple oxidation states. RuO_2 is expensive for commercial electrodes, so dispersion of RuO_2 in CNTs is a less expensive method of

manufacturing electrodes. The previously mentioned advantages of employing CNTs in electrochemical capacitors still apply in electrodes built in this fashion.

In 2003, Arabale *et al* [48], reported capacitive properties of MWNTs functionalized with ruthenium oxide (RuO_2). High purity aligned MWNTs were synthesized through the catalytic decomposition of a ferrocene-xylene mixture at approximately 675 C in a quartz tube reactor and over quartz substrates(CNT#6) [16]. The produced samples were refluxed with 6M nitric acid solution at 120 C for 3 hours to remove the metal catalyst impurities and generate oxygenated functional groups. The oxidized MWNTs were dispersed in isopropanol and water (1:1 volume) solution by ultrasonic agitation, to which $RuCl_3.3H_2O$ was added (1:0.5 MWNT : Ru wt ratio). The Ru/MWNT was filtered, washed with double distilled water and was dried in an oven at 110 C. A drop of the solution prepared by dispersing 3 mg of the dried Ru/MWNT mass in N,N dimethylformamide (DMF) was put on a glassy carbon electrode and dried under IR lamp. A three electrode assembly with Pt foil as counter and Ag/AgCl as reference electrode in 1 M H_2SO_4 was used to study the capacitance properties of Ru/MWNT electrode by cycling voltammetry, galvanostatic discharge and impendance spectroscopy techniques. The obtained value of specific capacitance was 80 F/g, compared to 30 F/g capacitance of pure MWNT electrodes.

A recent study in 2006 by J-K Lee and O-S Joo *et al* [49] proposed a different preparation method of Ruthenium oxide functionalized CNT electrodes and demonstrated an enhancement in the specific capacity up to 628 F/g. Initially a solution of 0.05 M $Ni(NO_3)2.6.H_2O$ is sprayed on a graphite working electrode and then the electrode is dried in an oven for 30 min at 100 C. Nickel salts on the electrode are decomposed under argon flow of 100 sccm for 2h at 600 C, and then reduced by hydrogen for 1h at 600 C. Then CVD method is employed via decomposition of acetylene under 1 atm of pressure for 3 minutes at 600 C in a tubular quartz reactor. The total flow to the reactor was 100 sccm with a ratio of acetylene to hydrogen of 1 to 9. Once the MWNTs (CNT#7) are formed on the electrode, they were impregnated with a ruthenium nitrosyl nitrate solution, followed by calcination at 350 C for 30 minutes. The electrode assembly as in

the previously mentioned work of Arabale *et al* is employed for determination of capacitance values for different weight fractions of RuO_2. The as grown MWNTs did not wet even in strong acid and base solutions. After treatment with piranha solution the wettability as well as specific capacity of MWNTs increased significantly (from 10 F/g to 100 F/g) The mentioned value of high specific capacitance of 628F/g was obtained when the weight ratio of MWNT to RuO_2 was 1.0 to 0.5.

Other than ruthenium oxide, nickel and manganese oxides were also used to enhance the capacitance properties of CNTs. In 2005, J. Y. Lee and Y.H. Lee *et al* [50] demonstrated that, nickel oxide/ CVD synthesized MWNTs (obtained from Iljin Nanotech, Korea, i.e.CNT#8) composite electrodes (10 wt% NiO) showed a specific capacitance of 160 F/g in a two electrode assembly with an electrolytic solution of 2M KOH without any noticeable decrease after 100 cycles. This is a significant increase when compared to when the electrode is only composed of CNTs, 45 F/g.

Chen *et al* in 2006 [41] studied manganese oxide/ MWNTs composite electrodes for their supercapacitive behaviors. The CNTs (CNT#9) are grown directly on graphite substrate using a simple catalyst prepared by electrochemical deposition followed by CVD in a furnace. They showed that the specific capacitance decreased from 568 F/g by only 12 % after 2500 cycles, measured in a typical three electrode cell with electrolytic solution of 1M Na_2SO_4. Table 2.5 below summarizes the capacitances and cell configurations of all the metal oxide/ CNT composites.

Table 2.5 Specific capacities of various metal oxide/ CNT composites

Metal Oxide - CNT composites	Specific capacity (F/g)
CNT#6	30
CNT#6/RuO_2	80
CNT#7	10
Piranha treated CNT#7	100
CNT#7/RuO_2	628
CNT#8	45
CNT#8/ NiO	160
CNT#9/MnO	568

Chapter 3 : Experimental Methods and Materials

In this Chapter the details of the thermal chemical vapour deposition (CVD) setup, the related experimental procedures , the choice of substrate types as well as the equipment and methods used for characterizing the synthesize CNT-metal composites are presented.

3.1 Thermal Chemical Vapour Deposition (CVD) Reactor Setup

As discussed in Chapter 2, the thermal CVD reactor involves the dissociation of a carbon containing gas through the use of thermal energy only, to produce carbon nanotubes (CNT) on substrates containing transition metals as catalysts. The main component of the CVD reactor is the heating source, itself. The heating of the reactor in this project is achieved by a tubular furnace which can be seen as in Figure 3.1a. The simplified schematic of the setup can be found in Figure 3.1b.

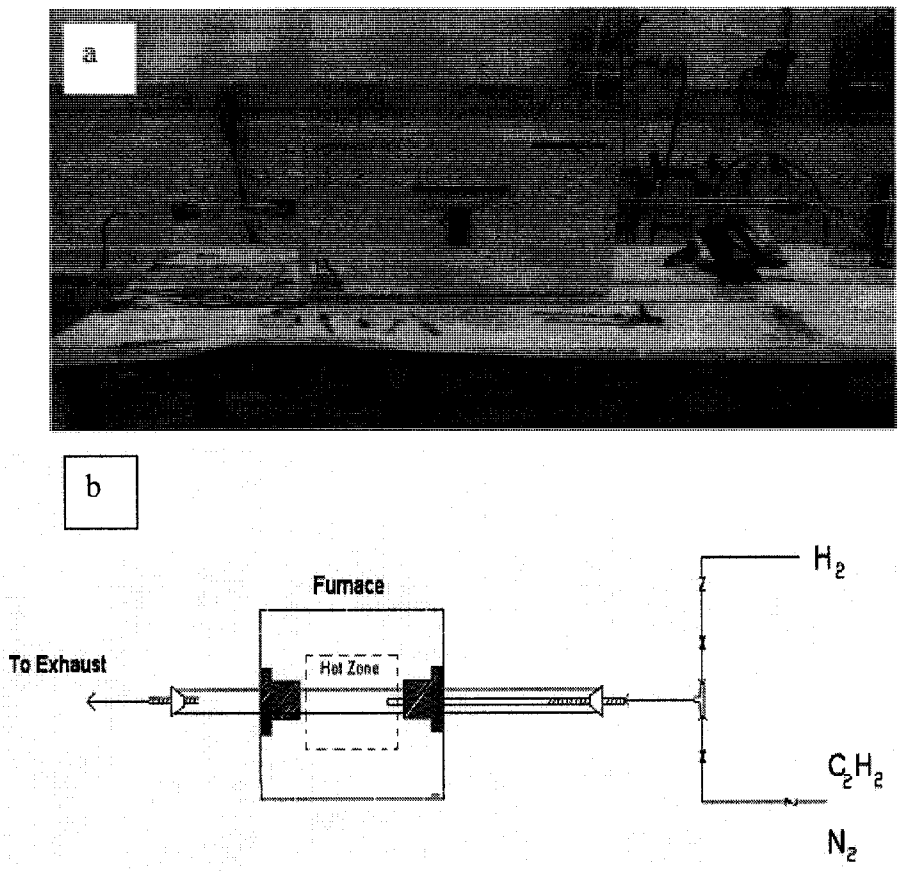

Figure3.1 The thermal CVD setup: a) photo b) schematic

The tubular furnace employed in this project is a Linderberg/Blue HTF series which can reach a maximum temperature of 1200 °C. A quartz tube of 4 feet in length and 2 inches in internal diameter is used as the reactor. The tube is placed inside the furnace so that approximately half of its length is in the heating zone. Silicone rubber stoppers at both ends of the tube are used to seal the tube. Steel tubes of 1/4" diameter are pierced trough the silicon rubbers to facilitate as inlet and outlet for the precursor gas mixture.

The precursor gas mixture is composed of acetylene (C_2H_2) as the carbon source and nitrogen (N_2) as the carrier gas. The mixing and adjustment of flowrates of the gases were achieved by a Matheson's model 7300 series proportioner and mixer. The gases are introduced into the hot zone through the use of a smaller glass tube (18 inches in length and 1/4 inches in diameter) and which is connected to the 1/4" steel tube. It is essential to introduce the gas mixture to the hot zone to avoid decomposition of C_2H_2 at lower temperatures observed in sections of the tube outside the furnace.

Large substrates are placed in the centre of the hot zone directly on the quartz tube whereas for positioning of smaller substrates a ceramic boat is employed.

3.2 Substrates

Various substrates and catalyst materials can be used to achieve CNT synthesis as described in Chapter 2. For the scope of this project it was desired to produce carbon nanotubes directly on metals, thus creating a direct chemical bond of CNTs; which are the active materials in supercapacitor applications with the metal as the current collector. The most common catalysts for CNT growth are transition metals such as Iron (Fe), Nickel (Ni) and Cobalt (Co). The metals employed in this project were copper, nichrome (60 wt% Ni, 16 wt% Cr and 24 wt% Fe) and stainless steel 304 (18 wt% Cr, 8 wt % Ni and 74 wt% Fe).

Even though copper is an excellent conductor, thus a significant current collector, it does favour CNT growth. Therefore, copper grids were electroless plated with nickel. The activation solution and electroless nickel plating bath conditions and compositions are found in the Table 3.1 given below [50]. The electroless nickel plating time was varied between 30 seconds and 2 minutes.

Table 3.1 Conditions and compositions for activation solution and electroless nickel plating bath for copper samples

Activation solution composition	
Paladium chloride (Cl_2Pd)	0.01 g
Hydrochloric acid (HCl)	1 ml
Water (H_2O)	100 ml
Electroless nickel plating composition and conditions	
Nickel chloride ($NiCl_2.6H_2O$)	9 g
Sodium hypophosphite ($NaH_2PO_2.H_2O$)	2.75 g
Sodium citrate ($Na_2C_6H_5O_7.2H_2O$)	25 g
Ammonium chloride (NH_4Cl)	12.5g
Water (H_2O)	250 ml
pH	8.5 - 9
Temperature	90 - 100
Buffering agent	Ammonium hydroxide

For electrochemical characterization purposes, all the metallic substrates were chosen to be in the form grids with varying mesh sizes (i.e. 40 x 40 and 400 x 400). The higher surface area available in a grid compared to a coupon or a plate was the decisive factor. All the metallic grids were purchased from McMaster-Carr. The sizes and shapes of the grids were varied depending on the characterization technique. The details of the geometries of the grids will be discussed later in their respective characterization methods.

3.3 Experimental Procedure and Conditions

The synthesis of CNTs on metallic grids was achieved generally via the conditions presented in the previous work of Reddy [51]. Slight modifications to his procedure were made in order to enhance CNT growth.

3.3.1 General CVD process

1. All the purchased grids are cleaned with acetone in ultrasonic bath for 20 minutes.
2. Nichrome and Stainless Steel 304 substrates are etched in an acid bath for varying times (0 – 5 minutes). Copper grids are electroless plated with Nickel.
3. The substrates are placed in the hot zone of the furnace and the air is purged from the reactor by the introduction of nitrogen at a flowrate of 1140 ± 5 sccm for 20 minutes to avoid oxidation of metal samples when the reactor is heated up.
4. The nitrogen flowrate is reduced to 570 ± 5 sccm. The furnace temperature is raised to a desired value of 700 °C and the system is allowed to equilibrate for 15 minutes.
5. Acetylene is introduced into the reactor at a flowrate of 45 ± 5sccm for 5 minutes.
6. The acetylene flow is stopped and the samples are kept at that synthesis temperature for another 30 minutes. This processing step is required to favour recrystallization of the CNTs.
7. The furnace is turned off and the reactor is allowed to cool down under a reduced nitrogen flow of 210 ± 5 sccm.
8. Once the reactor is cooled down to temperatures less than 70 °C, it was safe for the samples to be taken out.
9. In order to make sure no residual carbon deposited on the walls of the reactor affected the next experiments, the reactor was opened to air and the furnace was set to a temperature of about 650 °C to burn off the carbon residue.

3.3.2 Heat Pre-treatment prior to CNT synthesis

A heat pre-treatment method was employed prior to synthesis. Before setting the synthesis temperature for CNT (step 4 in the general experimental procedure), the samples inside the reactor are heated to elevated temperature of 850 °C and the system is allowed to equilibrate for 30 minutes. This treatment is known to allow precipitation of chromium along the grain boundaries in stainless steel samples causing iron and nickel to be more exposed [52].

After the pre-treatment, the reactor is brought back to the desired synthesis temperature and allowed to stabilize for 15 minutes prior to introduction of acetylene for CNT synthesis.

3.4 Characterization methods

The samples obtained from the thermal CVD process are characterized for their CNT content, morphology of the CNTs, surface area and electrochemical capacitance by the methods discussed below.

3.4.1 Field Emission Scanning Electron Microscopy (FE-SEM)

A FE-SEM *Hitachi* 4700 model was used to assess the CNT content of the samples, qualitatively. To image the samples, the metallic grids were cut to rectangles of size 1.5 cm by 1.0 cm and were anchored on the stainless steel support by carbon tapes. The FE-SEM was operated at 5.0 kV of accelerating voltage and 10 μA (or 20 in some cases) of emission current. The magnification was varied generally between 1,000 X to 60,000 X. The surface coverage by CNTs was calculated by an image analysis software called *ImageJ.*

3.4.2 Ultra-micro balance

The mass of carbon deposited on the metallic grids were obtained by a *Sartorius S4* Ultra-Micro balance. The minimum value the equipment can detect is 0.0001 mg, thus making it possible for determination of even minute quantities of carbon deposited.

3.4.3 Brunauer, Emmett and Teller (BET) Single Point Surface Area Analysis

A Flowsorp II 2300 model from *Micromeritics* is employed to determine both the combined surface area of CNTs on metallic grids and the CNTs only. The grids are cut to sizes of approximately 3mm by 3mm and gathered to weigh around 0.3 to 1 g depending on the mesh size of the sample. The samples are placed in a quartz sample holder and degassed at 200 °C for 1 hour in order to remove any gases that might have been adsorbed on the surface. Consequently a mixture of helium and nitrogen (70 mol % He, 30 mol% N_2) is passed through the sample and adsorption of N_2 on to the sample is achieved at 77 K by immersing the sample holder in a liquid nitrogen bath. Once the adsorption is complete, the value of the BET surface area (m^2) is calculated from the amount of gas desorbed as explained in Chapter 2, following the immersion of the sample holder in a water bath at room temperature. In order to determine the increase in specific surface area (m^2/g) the grids are weighed and analysed in Flowsorp II 2300 prior to and after the thermal CVD process. The change in surface area is divided by the change in the mass of the sample (i.e. mass of carbon materials deposited) to give the specific surface area of CNTs produced, $S_{BET\ spec.}$

3.4.4 Raman Spectroscopy

A *Renishaw inVia* Raman spectrometer was used to characterize the samples obtained from the thermal CVP process. The grids with CNTs are placed on a glass lamellae and a laser beam of 488 nm is focussed on the sample. The measured Raman spectra contain D, G and G' peaks as discussed in Chapter 2. The intensities of D and G' peak are used to calculate the $I_{G'} / I_D$ ratio which is used to assess the quality of the produced samples.

3.4.5 Electrochemical Capacitance measurement

Autolab Potentiostat / Galvanostat model 30 from *EcoChemie* is used to determine the capacitance of the samples obtained from the thermal CVD process by cyclic voltammetry (CV) measurements. A conventional three electrode cell is constructed with the sample as the working electrode, a platinum wire as counter electrode and a mercury/mercurous sulfate electrode (MSE) as reference electrode. The metal grids cut to a specific shape and the 3 electrode cell assembly are shown in Figure 3.2. The samples were tested in an aqueous environment in a 1M H_2SO_4 solution. Prior to the measurement of the CV, the system is purged off oxygen by bubbling argon for 30 minutes. Consequently, the samples are treated at a scan rate of 500 mv/s for 500 scans to make the CNTs more hydrophilic. CV is measured at varying scan rates (50 mv/s to 500 mv/s) and capacitance [F] (or specific capacitance, [F/g]) is calculated from the obtained CV as explained in Chapter 2.

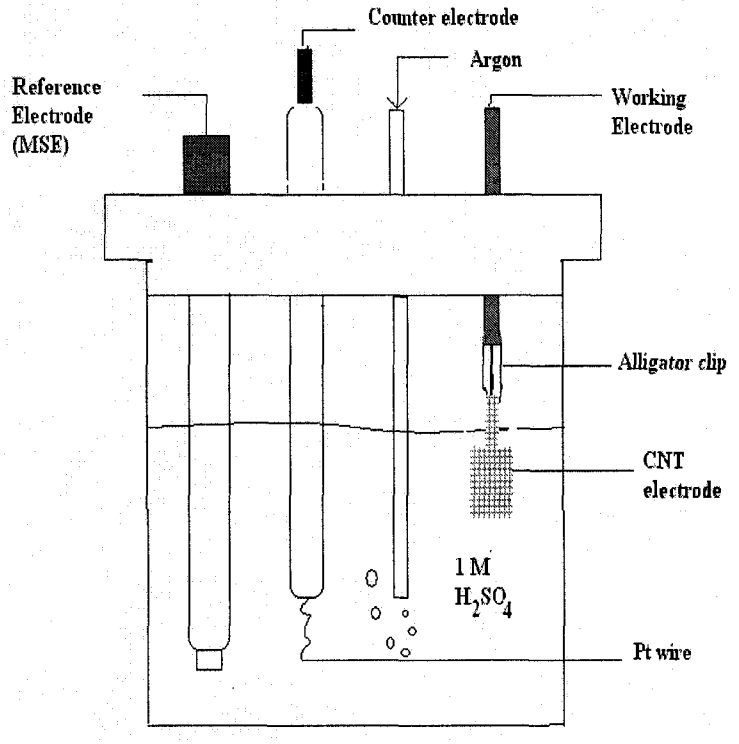

Figure 3.2 Schematic showing the 3 electrode cell assembly employed in measuring CVs of prepared CNT-metal composites.

Chapter 4 : RESULTS AND DISCUSSION

In this Chapter the results obtained from various characterization methods mentioned in the previous Chapter are presented and discussed. The Chapter is divided into two major sections: 1) Physical and 2) Electrochemical characterization. The physical characterization of the samples is achieved extensively with FE-SEM images and includes mostly qualitative observations. The electrochemical characterization includes the cyclic voltammetry results of samples produced.

4.1 Physical Characterization

The physical characterization of substrates is achieved by FE-SEM and *Image J* image analysis software to determine percent coverage (% coverage), ultra-micro balance to determine the amount of carbon materials synthesize, Raman Spectroscopy to calculate the $I_{G'} / I_D$ ratio to verify the presence of CNTs and assess the quality of the samples and finally BET surface area analyzer to measure the surface areas of the samples.

4.1.1 Quality and Yield of CNTs Synthesized on Metallic grids

As mentioned previously in Chapter 3, three types of metals are used to grow CNTs on : 1) electroless nickel plated copper (ENiCu), 2) Nichrome (Nich) 3) Stainless steel 304 with 2 different mesh sizes 40 and 400 (SS304-40 and SS304-400). Finer grids of the nichrome alloy however were not available. The samples were placed inside the thermal CVD reactor to produce CNTs at a synthesis temperature and time of 700 °C and 5 minutes respectively.

Untreated metallic grids

As is mentioned previously in this thesis, the most common metal catalysts used for CNT growth are iron, nickel and cobalt. Most of the techniques used in the literature involve sputtering or lengthy chemical / electrochemical methods to deposit particles of these metals on substrates. In order to keep this step simple it was decided to use

electroless plating of copper with nickel. The plating time was varied between 0.5 to 2 minutes. For most of the ENiCu samples obtained after the CVD process, it was obvious even to the naked eye that the nickel layer formed was not stable during the thermal CVD process. This layer was seen to peel off on large areas of the sample. The best results were achieved for samples plated for 1 minute and Figure 4.1a shows this rare case. Generally the imaged sample showed no growth as showed in Figure 4.1b.

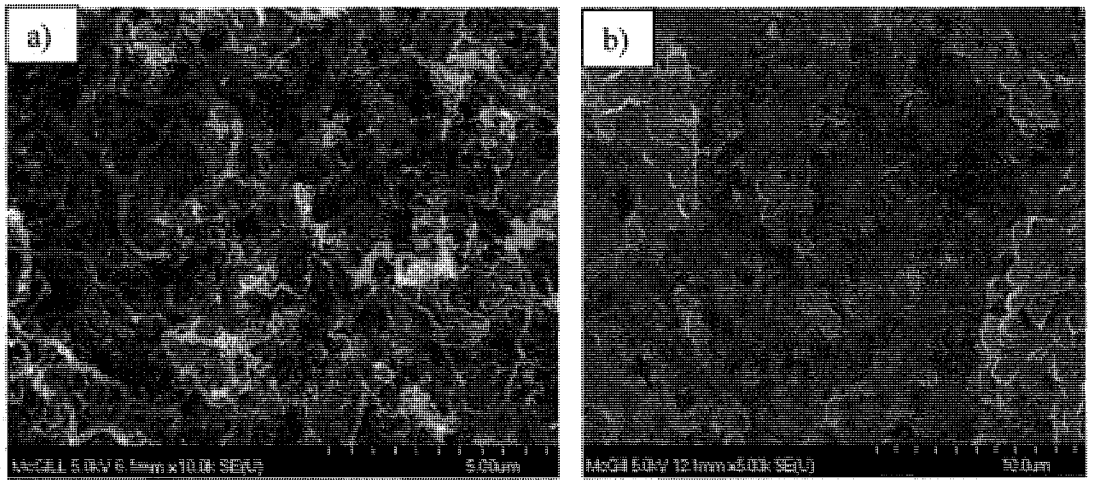

Figure 4.1 FE-SEM images showing a) Carbon fibers grown on ENiCu (1 minute in plating bath) b)no carbon growth on ENiCu

As observed from Figure 4.1a, the surface of the substrate is densely covered with carbon nano-fibers(CNF) of diameters in the range of 100 to 170 nm and a very small percentage contains CNTs with diameters in the range of 40 to 70 nm. As shown in Figure 4.1b, the nickel layer is easily removed during the CVD process. The removal of the nickel layer can be due to the rapid heating rate of the furnace (approx. 40 °C /min) The weak attachment of the catalyst surface to the copper base can also explain why there is a preferred formation of CNFs to CNTs. The diameters of ordered carbon structures such as CNTs relate highly to the size of metal catalyst particles available on the substrate. If the layer formed is loosely attached, then the heat treatment during the CVD process will not result in nanosized grains of metal particles (or as observed in most cases it will cause peeling of the layer completely) but rather larger grains. These larger sized grains might be the cause of CNF growth rather than CNTs.

Once it was established that electroless plating of copper with nickel was not suitable for CNT growth, it was decided to search for a material which already contained one or a combination of the metal catalysts to avoid a lengthy preparation step. Grids with the same mesh sizes (40 x 40) of a nickel chromium alloy called Nichrome (Nich) and Stainless Steel 304 (SS304-40) were decided to be used as the substrate materials to study the CNT growth.

For the same CVD synthesis conditions as for the ENiCu case, Nichrome samples without any chemical pre-treatment, showed a considerable increase in the amount of CNTs produced.

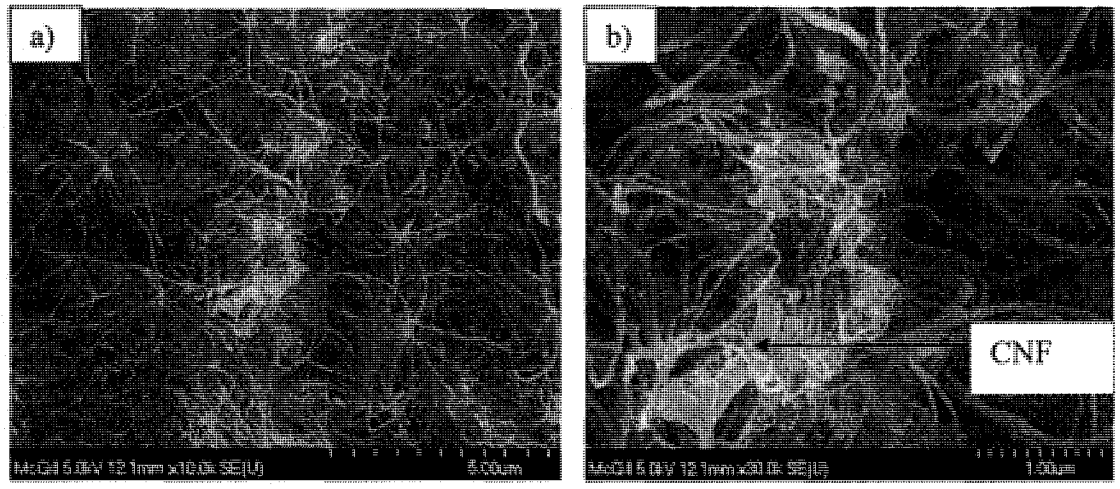

Figure4.2 FESEM images of Nichrome after thermal CVD process : a) lower magnification of 10 000 X b)higher magnification of 30 000 X

Figure 4.2 shows the surface of the substrate being covered densely and uniformly with CNTs. The diameters of the CNTs produced range from 15 nm to 80 nm, with the majority of the diameters being in the 60 to 80 nm range. It is also evident from the figure on the right that CNFs are also produced within the CNT matrix. The sample shows no visible amorphous carbon content suggesting that employing nichrome as the substrate yields a high quality product.

Similarly to the Nichrome sample, samples of SS304 also show considerable amount of CNT growth (Figure 4.3). Again in this case the diameters of the CNTs

produced lie in the 20nm to 80nm range and a few CNF are visible with almost no amorphous carbon. It can be hypothesized from these observations, that the heat treatment at 700 °C is responsible for the formation of nano-scale grains which induce CNT growth for metallic alloys.

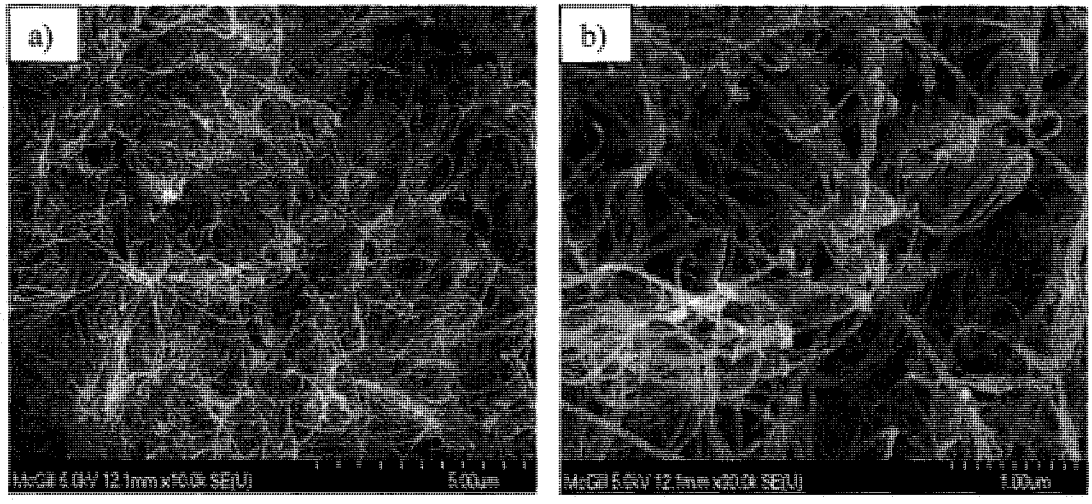

Figure 4.3 FESEM images of SS304 after thermal CVD process : a) lower magnification of 10 000 X b)higher magnification of 30 000 X

Even though the quality and content of CNTs might be similar in both cases, the CNTs tend to grow more densely and closely packed on the SS304 compared to Nichrome. This observation is more clearly illustrated when the images are analyzed at a lower magnification as shown by the images in Figure 4.4.

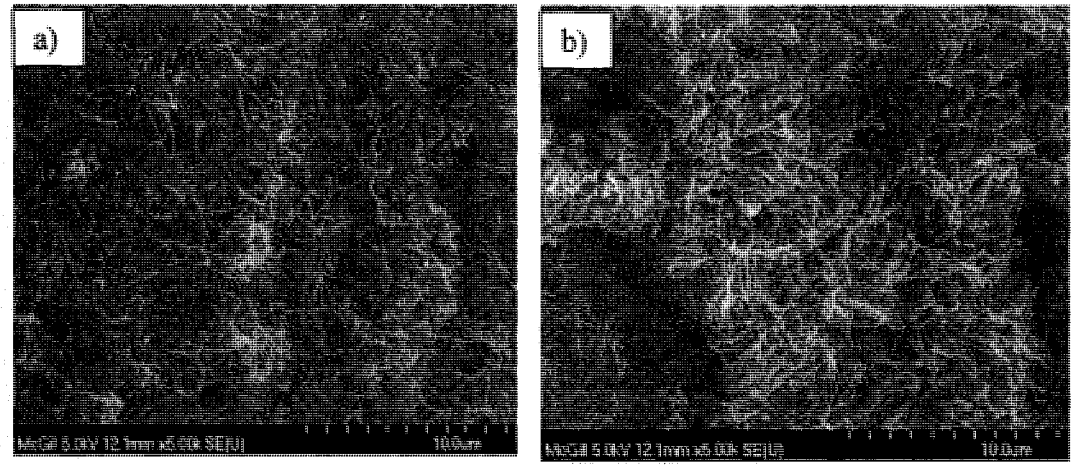

Figure 4.4 FESEM images comparing the CNT growth on a)Nichrome b) SS304 at a magnification of 5000 X

This observation is also reflected on the amount of CNTs synthesized following the thermal CVD process. About 1 ± 0.3 mg of CNTs are deposited on SS304 whereas this value is about 0.25 ± 0.1 mg for the case of nichrome with similar initial weights and geometrical sizes. Table 4.1 shows the differential change in mass before and after the CVD process for an experimental run observed for these two samples.

Table 4.1 Differential change in mass before and after CVD for Nichrome and SS304 for a CVD experiment

	WEIGHT of samples (mg)		
	before CVD	after CVD	Difference
Nichrome	80.3	80.5	0.2
SS 304-40	71.3	72.4	1.1

Although the quality and content of CNTs seemed reasonable for both alloys, it was necessary to obtain a sample which would yield higher loads of CNTs for better evaluation of the specific surface areas of these materials. A finer grid of SS304 having a mesh size of 400 x 400 of SS304 was also investigated (SS304-400). This finer grid structure provided smaller wire diameters than the previous one, and thus smaller initial weights for the same geometrical size of other types of grids studied. Table 4.2 below summarizes the initial weights and theoretical specific surface areas per square inch of grid samples. The related calculations can be found in Appendix I.

Table 4.2 Theoretical weight and specific surface areas of grids of 1 inch x 1 inch

Metal	Weight (g)	S_{calc} (m^2/g)
Nich	0.882	1.9×10^{-3}
SS304-40	0.84	2.0×10^{-3}
SS304-400	0.0824	2.0×10^{-2}

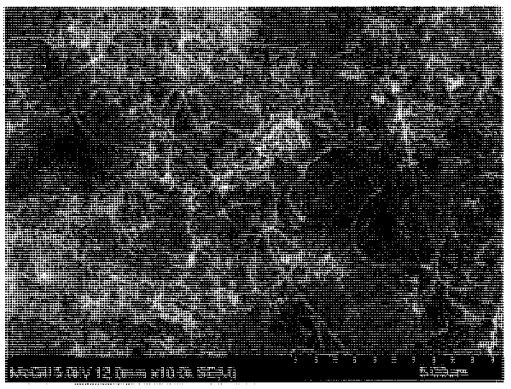

Figure 4.5 FESEM image of SS304-400 after thermal CVD process

In terms of CNT distribution and quality, the as received SS304-400 samples did not differ from the previously studied SS304-40 (Figure 4.5) ; however due to the fact that less metal catalyst by weight was present compared to the SS304-40 case, the total amount of CNTs deposited was only around 0.3 ± 0.1 mg for a sample weight of about 15 mg. A better comparison between the substrates is obtained when the amount of CNT synthesized is divided by the total weight of CNT-metal composite to obtain the fraction of CNT in the composite.

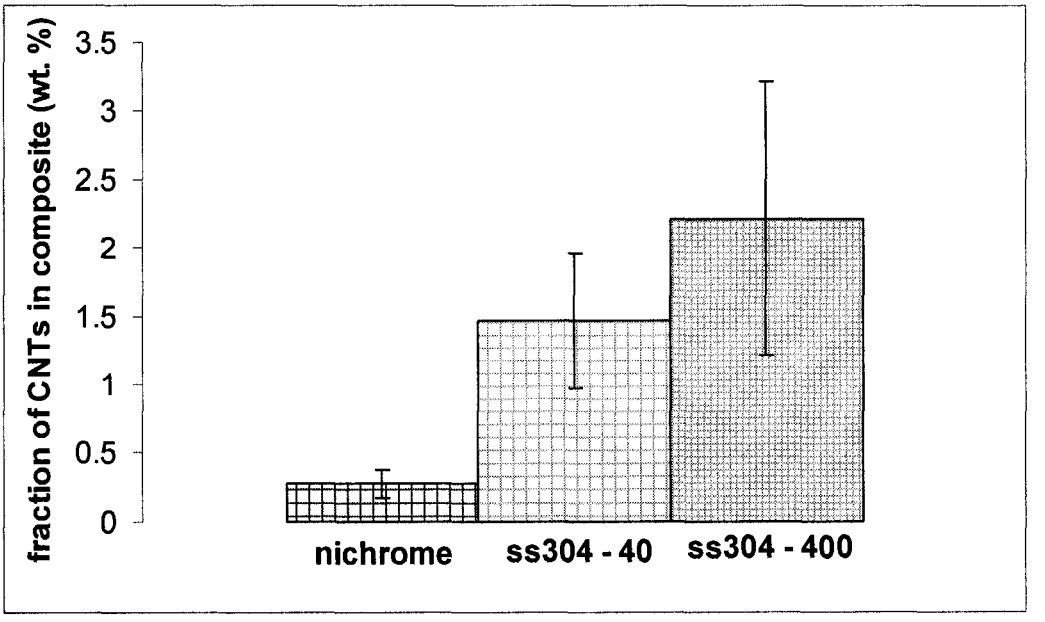

Figure 4.6 Bar chart comparing CNT to CNT-metal composite weight ratios of metallic grids used

As observed in Figure 4.6, the highest ratios are observed for SS304-400. The error bars are calculated from 8 samples for each type of metallic grid processed under the same CVD conditions. The magnitude of the error bars for SS304-40 and SS304-400 indicate that there is no significant difference in the amount of CNT present for these as received samples. Although the weight fractions obtained for stainless steel grids are significantly higher than nichrome grids, the fractions of about 1.0 to 3.0 % still needed to be improved.

Effect of acid treatment

In order to achieve higher CNT production, the stainless steel substrates were treated with hydrochloric acid (HCl) to etch away the protective oxide layer and increase the surface defects. This process was developed by Baddour at McGill University [53] in order to grow CNTs on polished stainless steel strips and it was reported that an etching time of 5 minutes was optimal. The two sizes of the stainless steel grids were treated with HCl for 2.5 and 5 minutes and weighed prior to the CVD process.

Figures 4.7 and 4.8 shows the FESEM images of CNTs grown on two sizes of SS304 grids treated with HCl for 2 different etching times. For an etching time of 2.5 minutes, amorphous carbon content on the surface of the SS304-40 (Figure 4.7 a) increased significantly compared to the as received SS304-40 samples (Figure 4.4). The CNT coverage of the surface was measured to be approximately 75 %. This phenomenon was not observed for the SS304-400 case (Figure 4.7 b). The etching of the finer grid resulted in thick CNT bundles even covering the spaces in between the grids (Figure 4.7 c).

The increase in the amorphous carbon content was even more pronounced for the SS304-40 case when the samples were treated with HCl for a longer time of 5 minutes (Figure 4.8 a). The surface coverage of CNTs was further reduced to approximately 45 %. The SS304-400 still showed a considerably high amount of CNTs, evenly distributed across the sample (Figure 4.8 b) but the rigid and lengthy bundles of CNTs are missing in this case when observed at a lower magnification (Figure 4.8 c). The surface coverage by CNTs is again very close to 100 %.

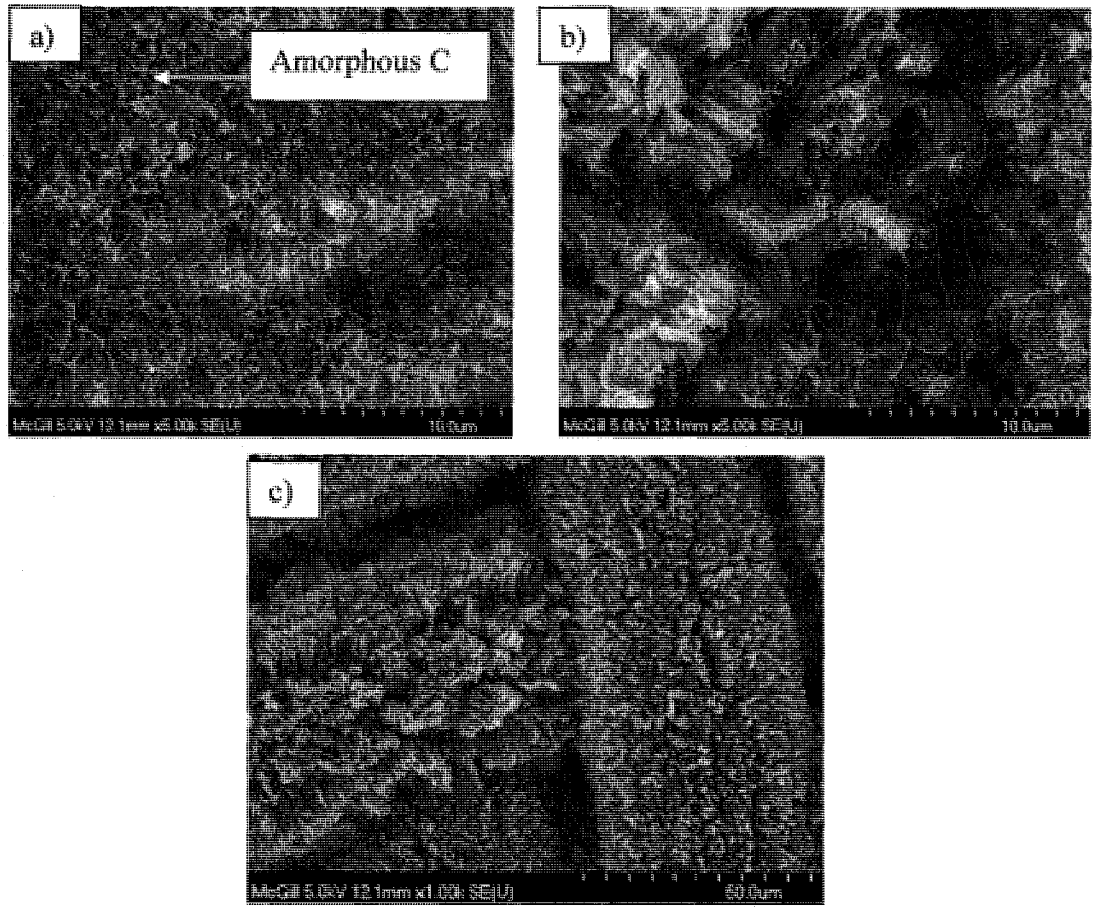

Figure 4.7 FESEM images of SS304 grids treated with HCl for 2.5 minutes prior to CVD: a) SS304- 40 b) SS304-400 c) SS304-400 at a lower magnification showing a more global coverage of the grid

In order to understand why the amorphous content was observed for SS304-40 but not for SS304-400 following the HCl treatment, the surfaces of the untreated grids were examined under the FESEM. The images observed in Figure 4.9 revealed that the SS 304-40 contained considerably more surface roughness and cracks compared to SS304 - 400. To study further this effect polished stainless steel strips were roughened with sandpaper and then treated with HCl for 5 minutes. Figure 4.10 clearly illustrates that for the roughened and HCl treated case almost all the surface is covered by amorphous carbon.

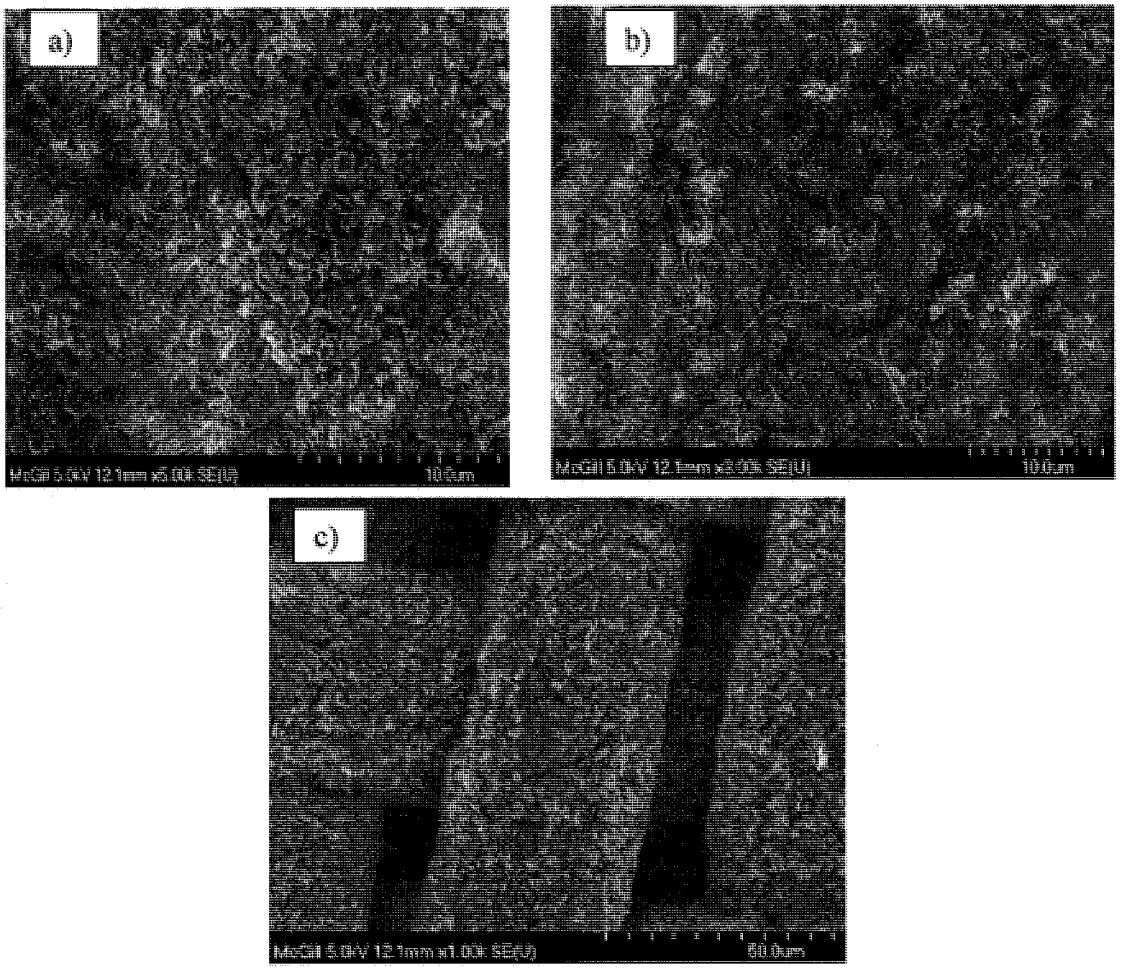

Figure 4.8 FESEM images of SS304 grids treated with HCl for 5 minutes prior to CVD: a) SS304- 40 b) SS304-400 c) SS304-400 at a lower magnification showing a more global coverage of the grid

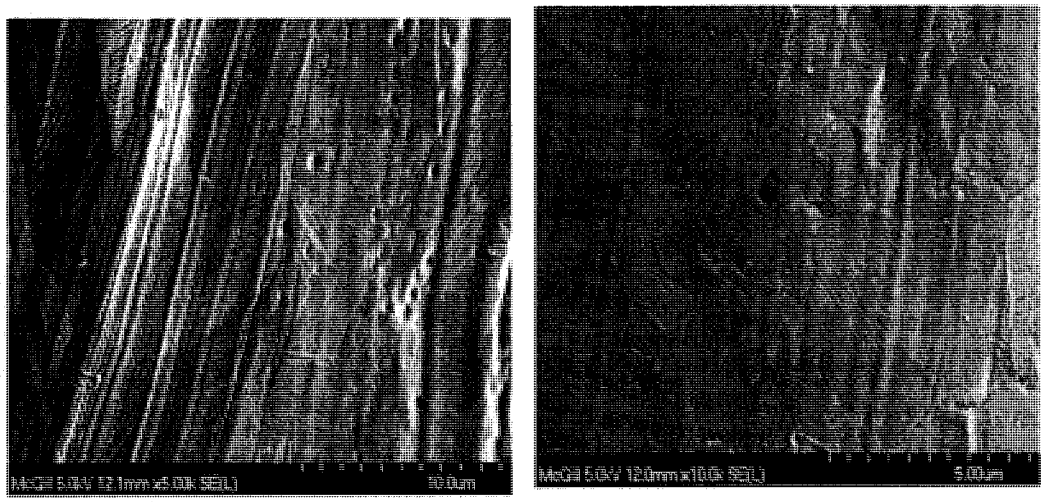

Figure 4.9 FESEM images of as received samples prior to HCl treatment and CVD process: a)SS304 – 40 b)SS304 – 400

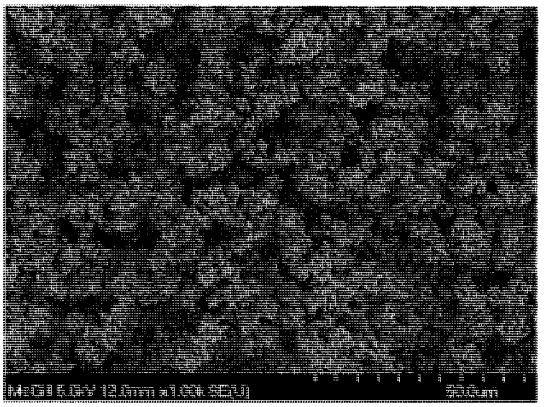

Figure4.10 FESEM image of a roughened and HCl treated SS304 strip after CVD process

It was concluded from these observations that for enhanced CNT growth it was not necessary for SS304- 40 to be treated with HCl. For SS304-400, HCl treatment for 2.5 minutes assisted in yielding long CNTs, densely packed together to form CNT bundles. The beneficial effects of HCl treatment to SS304-400 are also observed quantitatively when the weight fractions of CNTs in the composite are compared to the previous untreated cases as shown in Figure 4.11. The HCl treatment considerably influences the amount of CNT deposited on SS304 – 400. In the present study an HCl treatment of 2.5 minutes for SS304 – 400 provides the best conditions to produce CNTs.

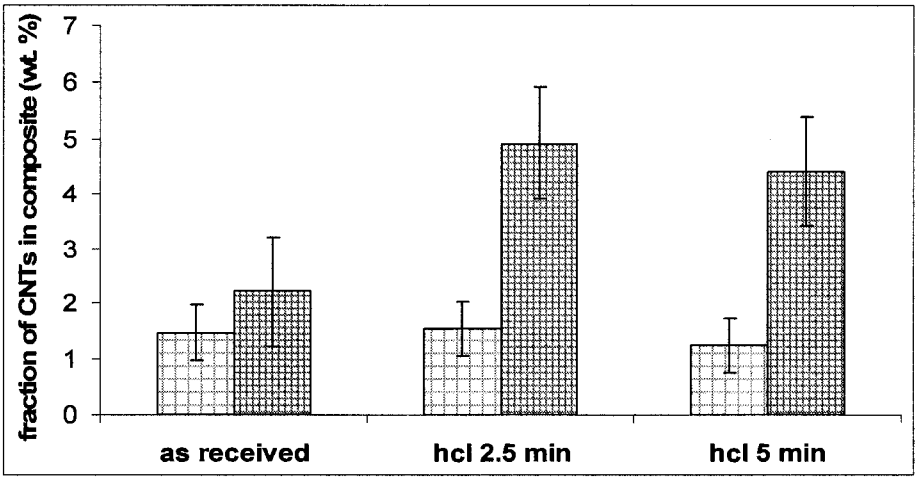

Figure 4.11 Bar chart comparing the fraction of CNTs in composites of as received and HCl treated stainless steel grids ☐ ss 304 - 40 ▦ ss 304 - 400

Effect of heat pre-treatment

As mentioned in Chapter 3, a heat pre-treatment method was also investigated to increase the CNT content on the grids. This pre-treatment method involves a simple heat treatment of the metallic substrates under nitrogen at a temperature of 850 °C prior to synthesis of CNTs. It is known that the chromium precipitates at the grain boundaries around this temperature for stainless steel samples, making the iron and nickel catalyst particles more attainable to the available carbon for CNT growth [52]. This process was evaluated using stainless steel strips by Baddour with promising results [53]. However, grid based experiments did not reproduce the results obtained on flat metal surfaces of the foils. The images of as received and HCl treated SS304-40 grids following this pre-treatment are given in Figure 4.12. Both samples show very little CNT production with the majority of the substrate surface being covered with amorphous carbon. Such a result may possibly be attributed to the microstructure differences for the two materials, the foils being generated by a rolling process while the grids wires should be produced by extrusion processes.

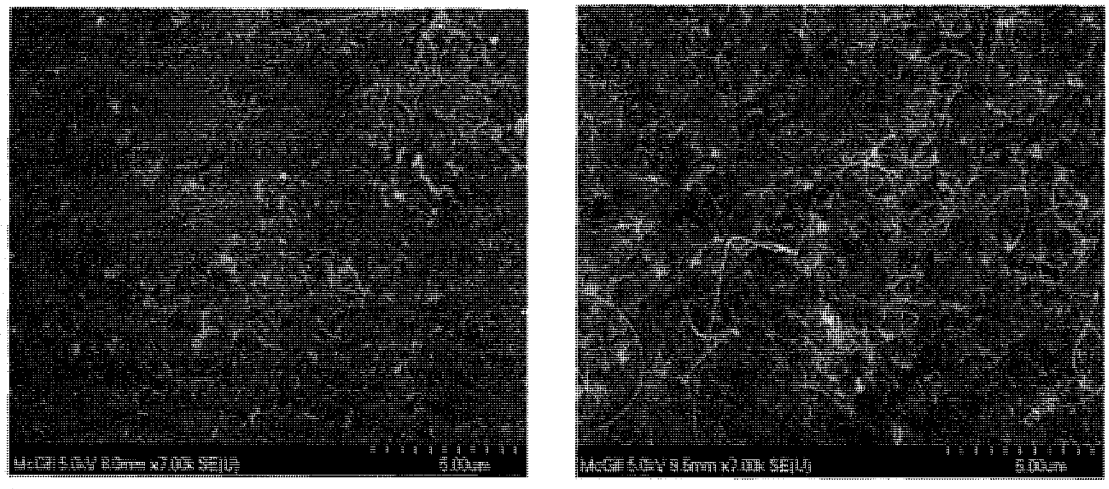

Figure 4.12 FESEM images of SS304-40 samples after a heat pre-treatment under Nitrogen at 850 °C : a) as received SS304-40 b) HCl treated SS304-40 for 2.5 minutes

4.1.2 Raman spectroscopy results

Raman spectroscopy was used to verify the presence of CNTs and assess the quality of the final product. The raman spectra for the two sizes of stainless steel grids are given in Figure 4.12, both treated with 2.5 minutes of HCl. As described in Chapter 2, the characterization of CNT samples are made trough the presence of 3 peaks : D (1250 – 1350 cm^{-1}) , G (1500 – 1600 cm^{-1}) and G'(2500 – 2800 cm^{-1}). The sharp D, G and G' peaks confirm the presence of MWNTs in both samples as observed in Figure 4.13. The slightly larger D peak and reduced G' peak observed for SS304-40 are the consequences of a higher amorphous carbon content.

Recently Raffaelle *et al* [36] found that the $I_{G'}$ / I_D ratio is the most sensitive to changes in MWNT purity and proposed the following equation to estimate the purity of a sample:

$$I_{G'} / I_D = 0.31 \exp(0.021X) \qquad (1)$$

where, X denotes the purity of the sample.

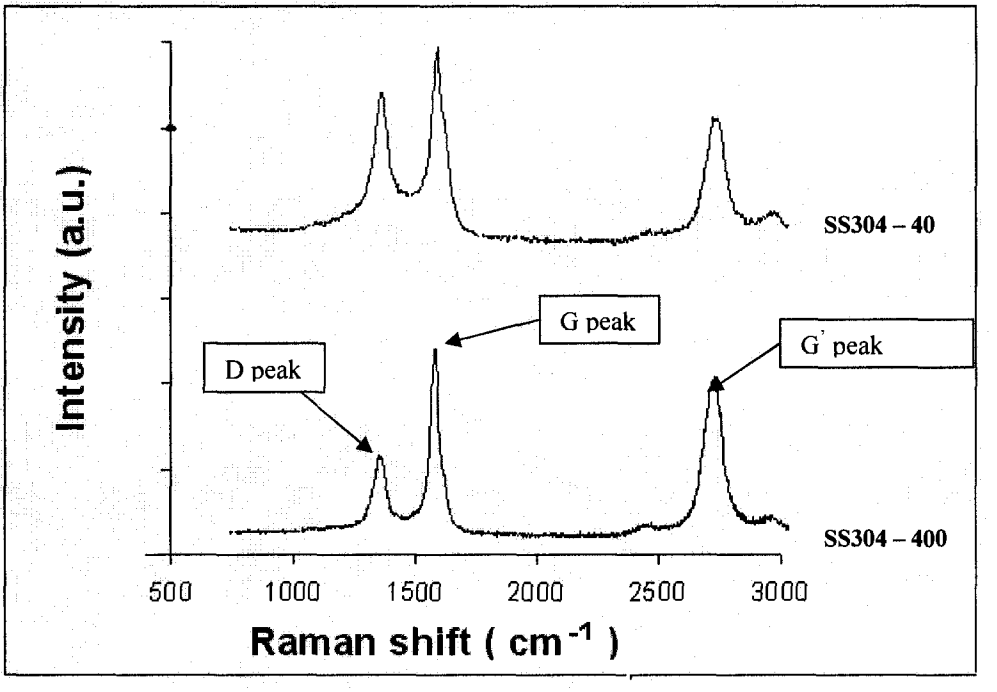

Figure4.13 Raman spectrum of SS304 -40 and SS304 – 400 treated with 2.5 minutes of HCl.

The purity values calculated for samples of SS304 – 40 and - 400 with and without HCl treatment can be found in Table 4.3. The values validate the observations made by FESEM images (i.e. highest CNT purity was found for SS304 treated with HCl for 2.5 minutes). It is important to note that even for the cases when CNT coverage of the surface was observed to be 100% by image analysis, the purity calculated by this method did not exceed 89 %. This result suggests that even though amorphous carbon was not visible in the FESEM images, it may have been dispersed within the thick CNT bundles.

Table 4.3 $I_{G'}$ / I_D ratios and purities of CNT- SS304 composites

Composite	HCl treatment	$I_{G'}$ / I_D	X (%)	% coverage
CNT-SS304-40	-	1.79	83	~ 100
CNT-SS304-40	2.5 min	0.84	47	~ 75
CNT-SS304-400	-	1.84	85	~ 100
CNT-SS304-400	2.5 min	2.01	89	~ 100

For the remainder of this chapter, SS304 – 400 will be used to denote SS-304 – 400 treated with HCl for 2.5 minutes, since it showed considerably better CNT yield and quality. The acronyms SS304-40 and Nich, still refer to the as received metal samples.

One should, however, be cautious in the use of Raman peak ratios as the values of peaks, particularly the D peak which results also from the presence of defects in the MWNT structure as well as the amorphous carbon structures. The ratio developed by Raffaelle *et al* [35] might show some dependence on the structure of the MWNT used in their study. Such structure is highly dependent on the growth process and growth conditions in a given process.

4.1.3 Single Point BET surface area of CNTs

It is a known fact that the electrochemical double layer capacitance depends on the available surface area of the material, therefore it was necessary to measure the surface area of the prepared CNT-metal composites. The surface area determination was achieved trough single point BET surface area analysis.

Degassing

Prior to any surface area measurement, it was necessary to evaluate the time required to degas the samples in order to eliminate any previously adsorbed gases in the pores of the samples, making the surface ready for adsorption of N_2.

A sample of purchased CNTs from Nano-Amor (80 % MWNTs) was used as the standard to determine degassing conditions. The degassing temperature was set to 200 °C and two experiments were conducted with 1 hour and 24 hours as the degassing time. The BET surface area measured for the same sample at those two conditions did not show any significant difference. It was decided to use only 1 hour as the degassing time for the produced samples. The specific BET surface measured for a sample of purchased CNTs was 86 m^2/g. The degassing conditions found for CNT powders are applicable to CNT-metal composites, since the metal composites contain CNTs at much lower quantities. If the degassing time was long enough to remove any gases from a CNT powder sample, it should also be able to degas the CNT-metal composites produced.

According to the specifications from the supplier of purchased CNT sample, the specific surface area is 200 m^2/g. In order to validate the value obtained, the same sample was tested in a recently purchased Tristar BET surface area analyzer from Micromeritics and a specific surface area of 91 m^2/g was measured. This result suggested that the surface area values obtained for the CNT powder by the surface area analyzer we had at our disposal could be trusted.

Comparison of specific surface areas of metallic grids

In order to determine the surface area of the produced CNTs only, it was necessary to measure initially the surface area of the plain grid surfaces and compare those to the surface area of the CNT-metal composites. The single point BET surface areas of the metallic grids are tabulated in Table 4.4. Due to the fact that nichrome and

SS304-40 grids are a lot heavier than SS304-400, the specific surface area for these materials are considerably lower.

Table 4.4. BET surface areas of metallic grids without CNTs

Metal	weight (g)	BET area (m^2)	specific BET area (m^2 /g)
Nich	1.23	0.14	0.11
SS304 -40	1.13	0.19	0.17
SS304-400	0.32	0.17	0.55

Comparison of specific surface areas for CNT-metal composites

As mentioned earlier, the weight ratio of CNTs to CNT-nichrome composite was significantly lower than both CNT - SS304 composites (Figure 4.6). The result of this would be a lower specific surface area for the CNT-nichrome composite. This is validated by the BET surface area analysis and compared to the values obtained for other types of composites as seen in Table 4.5.

Table 4.5 BET surface areas of CNT-metal composites

Composite	weight (g)	BET area (m^2)	specific BET area (m^2 /g)
CNT - Nich	1.23	0.22	0.18
CNT - SS304 -40	1.15	0.54	0.44
CNT - SS304-400	0.34	0.45	1.32

Specific surface area of CNTs produced on metallic grids

The specific surface area for CNTs only are calculated by dividing the difference between total BET surface area of CNT-metal composite and plain metal by the amount of CNTs produced. Table 4.6 includes these calculated values for each substrate. It is evident from the values that the specific surface area of the CNTs is independent of the material that they were synthesized on. As mentioned previously, the CNTs did not show significant morphological differences with different substrates, only the amount of CNTs synthesized differed. Therefore, it was expected to observe similar values for specific surface area. However, these values are significantly lower than the values obtained in

the literature (CNTs have specific surface areas generally in the range of 100 – 300 m^2/g). The BET surface area analysis relies on the adsorption/desorption mechanisms on porous powders. Thus, the surface areas measured for the samples, especially for the blank metallic grids, might not be representative of the real values. This would cause the surface areas of CNTs calculated to be lower than expected. The values obtained in this section will be compared to electrochemically active surfaces measured in the next section.

Table 4.6 BET surface areas of CNTs only

Composite	weight (mg)	Difference in BET area (m^2)	specific BET area (m^2 /g)
CNTs on Nich	3.7	0.08	21.6
CNTs on SS304 -40	17.2	0.35	20.3
CNTs on SS304-400	11.1	0.28	25.2

4.2 Electrochemical Characterization

Electrochemical characterization of the composites was achieved via cyclic voltammetry (CV) at varying scan rates [mv/s] in a 1 M sulphuric acid solution (H_2SO_4) as mentioned previously in Chapter 3. The potential window covered was 0 to 0.6 V. When the composites were introduced into the electrolyte, a film of air was trapped around the sample, verifying the high hydrophobicity of CNTs. This wetting problem was a major concern since electrochemical capacitance relies on the availability of ions to the pores in the active material, CNTs in this case. However, it was quickly observed that after about 500 scans at high scan rate of 500 mv/s, the film of air was removed and an increase in the current was observed. Figure 4.14 illustrates this situation. It is possible that the change in hydrophilicity is actually caused by the applied potential sweep. The growth of the double-layer in the liquid region along the surface (triple solid CNT/ air / liquid interface) might provide change in hydrophilicity. The CV of a CNT-SS304-40 sample at 500 mv/s is given in the mentioned figure. For comparison purposes, all the

samples were scanned for about 500 times and verification was made to ensure no further increase in current was observed prior to changing scan rates.

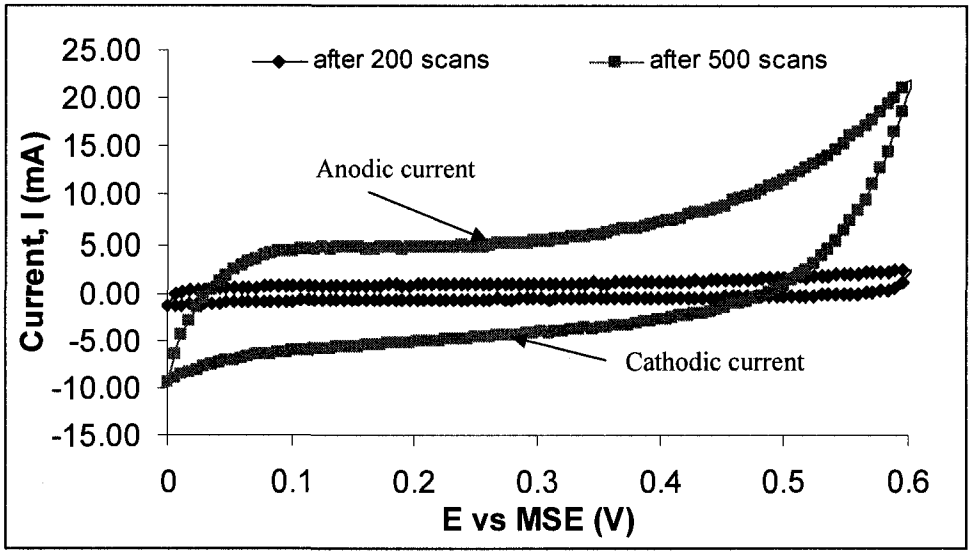

Figure 4.14 CV of a CNT-SS304-40 sample after 200 and 500 scans, showing the increase in the measured current.

CVs obtained at varying scan rates can be used to calculate the capacitance, C [F] for each composite as described in Chapter 2. For carbon materials, the double layer capacitance associated with the electrode aqueous solution interface has value between 15 and 50 $\mu F/cm^2$ [38]. Taking an average value of 25 $\mu F/cm^2$, the electrochemically active surface areas of the samples can be calculated by dividing the capacitance by this value. All the values calculated in this section are summarized in the Table 4.7 and are compared to values of surface area measured by the BET surface area analyzer. In order to investigate the increase in capacitance due to CNTs, CVs for blank metallic grids are also measured at a scan rate of 500 mv/s.

4.2.1 CNT-Nichrome composite

For typical electrochemical capacitor performance the CV of the sample should produce a rectangular curve across a chosen potential window. The CNT-Nich composite displays this expected behaviour as shown in Figure 4.15. The increase in capacitive current due

to increasing scan rate supports ideal electrochemical capacitor behaviour (Section 2.5.2). The plot in Figure 4.16, shows the dependence of anodic current taken at the midpoint of the potential window to scan rate. The cause for slight deviation from linearity observed at the smaller scan rates is unknown. It should however be noted that these results do not contain replicates due to the limited number of electrodes prepared. Statistically it is possible that if numerous electrochemical experiments were carried the data could present a better linear fit. With the data available it is assumed that linear relationship holds and the slope of the best fit is used to calculate the capacitance. Same situation is holds for the other composites as well. The value of capacitance obtained for this type of composite is 0.0071 F. Thus, the electrochemically active surface area is calculated to be 284 cm^2.

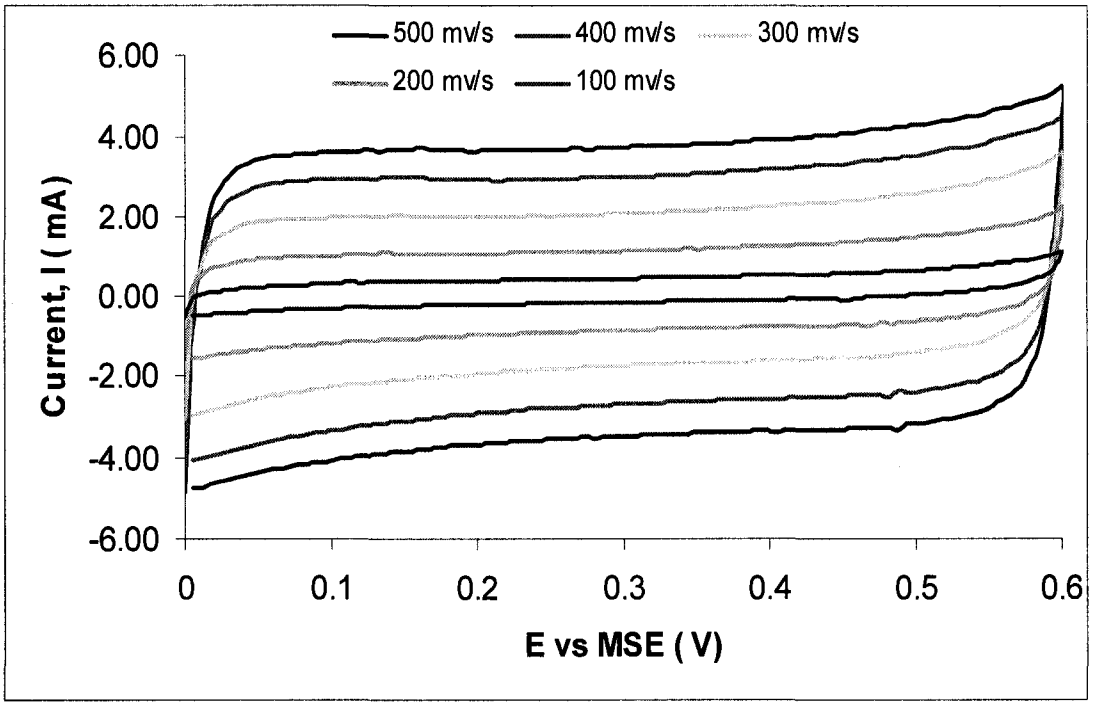

Figure 4.15 CVs of CNT-Nichrome composite at varying scan rates from 100 mv/s to 500 mv/s

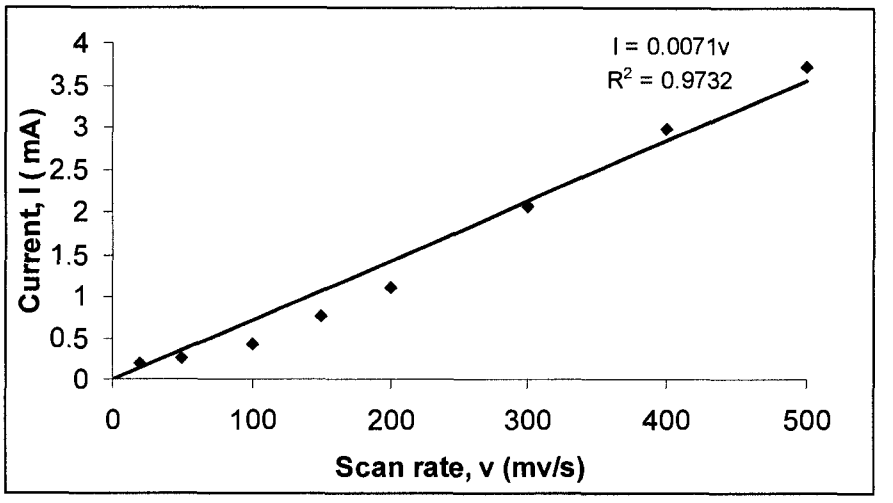

Figure 4.16 Dependence of anodic current at 0.3 V on scan rate of CV for CNT-Nichrome composite

In order to validate the effect of CNTs, the blank CV of this metallic grid is compared to that of the composite. To assess better the increase in capacitance, the current is divided by the weight of respective samples to give specific current, I_{spec} [mA/g] as seen in Figure 4.17. As it can be inferred from the mentioned figure, there is a considerable increase in the specific current, even though this substrate showed the least amount of CNT synthesis.

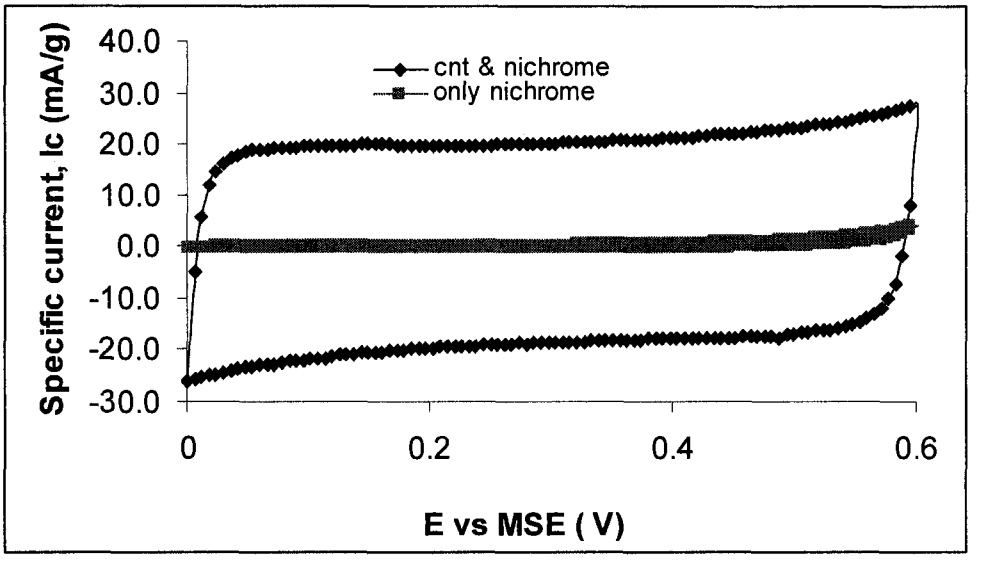

Figure 4.17 Comparison of CVs obtained for blank nichrome and CNT-nichrome composite at 500 mv/s

4.2.2 CNT-SS304 -40 composite

The CVs at varying scan rates for this composite is shown in Figure 4.18. The rectangular shape observed for CNT-nichrome composite is observed only up to 0.4 V, however the capacitive current measured still increases with increasing scan rates. The deviation from a rectangular shape might suggest pseudocapacitance effects since there is considerable delay of potential during reversing of the potential scan. This delay is connected with a kinetically slow process involved during charging the pseudocapacitance[39]. For our purposes, the area of high interest is the midrange of potential window, where the capacitive current is relatively constant.

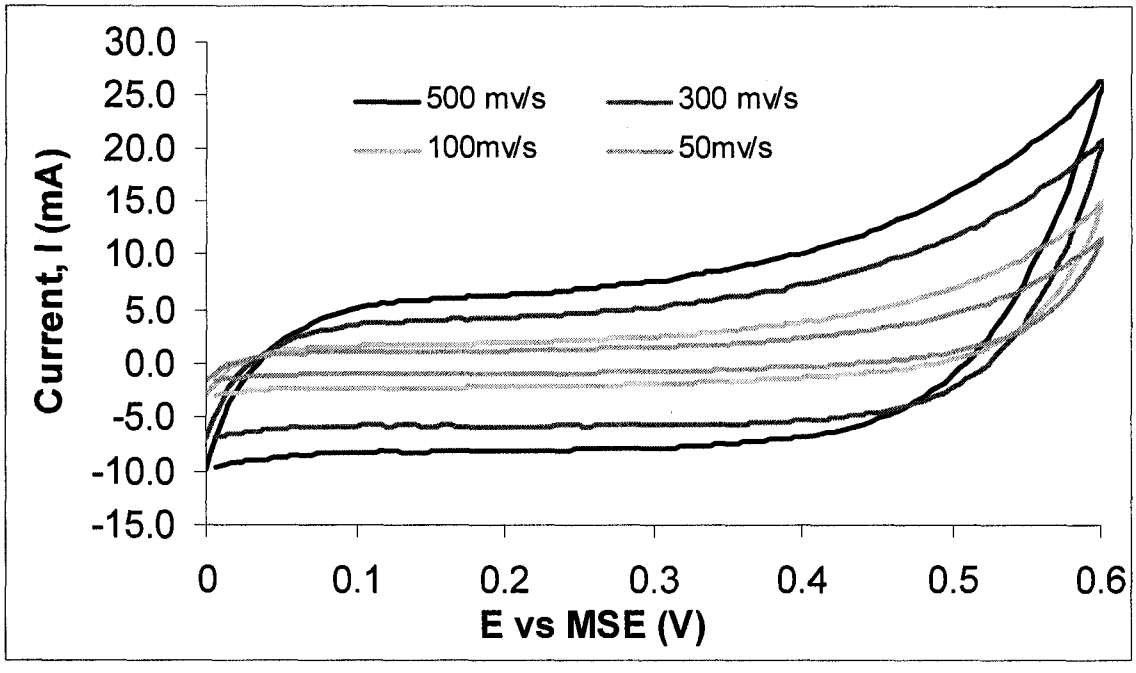

Figure 4.18 CVs of CNT-SS304-40 composite at varying scan rates from 50 mv/s to 500 mv/s

Similarly for the previous case the anodic current at 0.3 V is plotted against the scan rate in Figure 4.19 to calculate a capacitance value of 0.0168 F, resulting in an electrochemically active area of 672 cm^2.

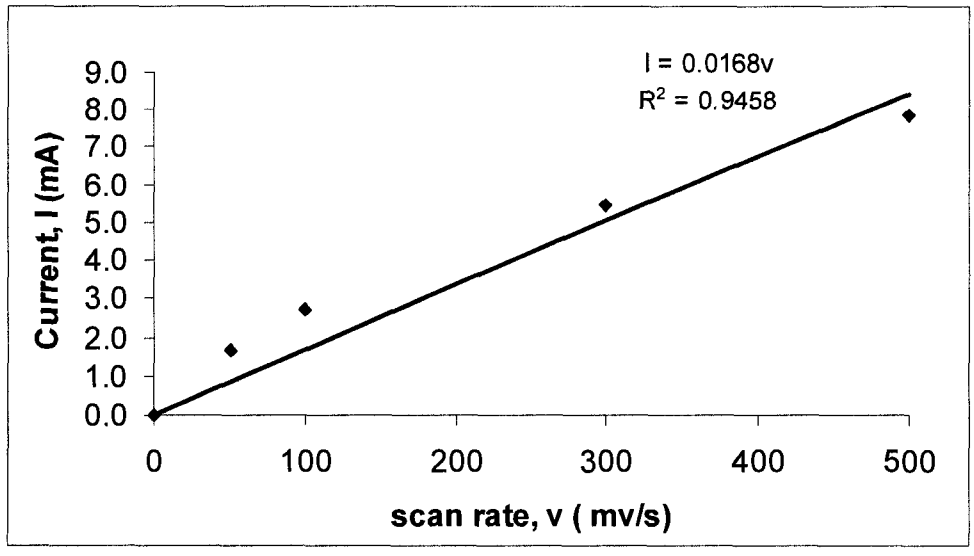

Figure 4.19 Dependence of anodic current at 0.3 V on scan rate of CV for CNT-SS304-40 composite

When the specific capacitive current (I_{spec}) for blank SS304-40 is compared to that of the composite again a considerable effect of the CNTs is visible from Figure 4.20. The values of I_{spec} measured in this case slightly larger than those observed for CNT-Nich composite. This increase in I_{spec} is mostly due to the fact that SS304-40 samples are less heavy. In addition, to that this substrate yields higher amounts of CNTs as mentioned previously, thus enabling higher capacitive current (I).

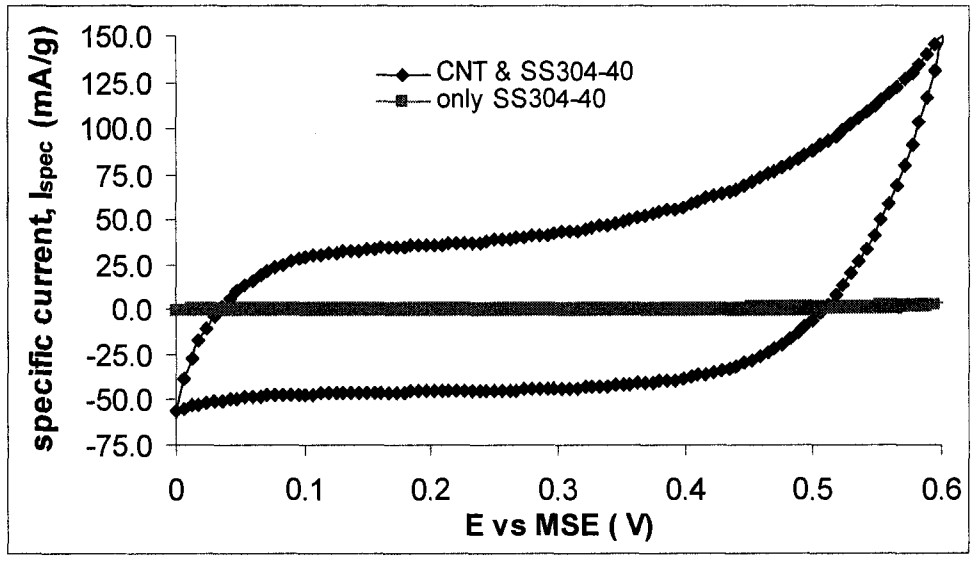

Figure 4.20 Comparison of CVs obtained for blank SS304-40 and CNT-SS304-40 composite at 500mv/s

4.2.3 CNT-SS304-400 Composite

Compared to the coarser grid, the CNT-SS304 – 400 shows a CV curve that is closer to the rectangular shaped observed for ideal electrochemical capacitors for the same potential window as observed from Figure 4.21. The visible peak around 0.1 V and the delay in potential during the reversal of the potential scan again suggest the possibility of pseudocapacitive behavior. The capacitance and the electrochemically active surface area are calculated to be 0.062 F (Figure 4.22) and 248 cm^2, respectively. The specific capacitive current reached for this sample is higher than those observed for the other composites (Figure 4.23).

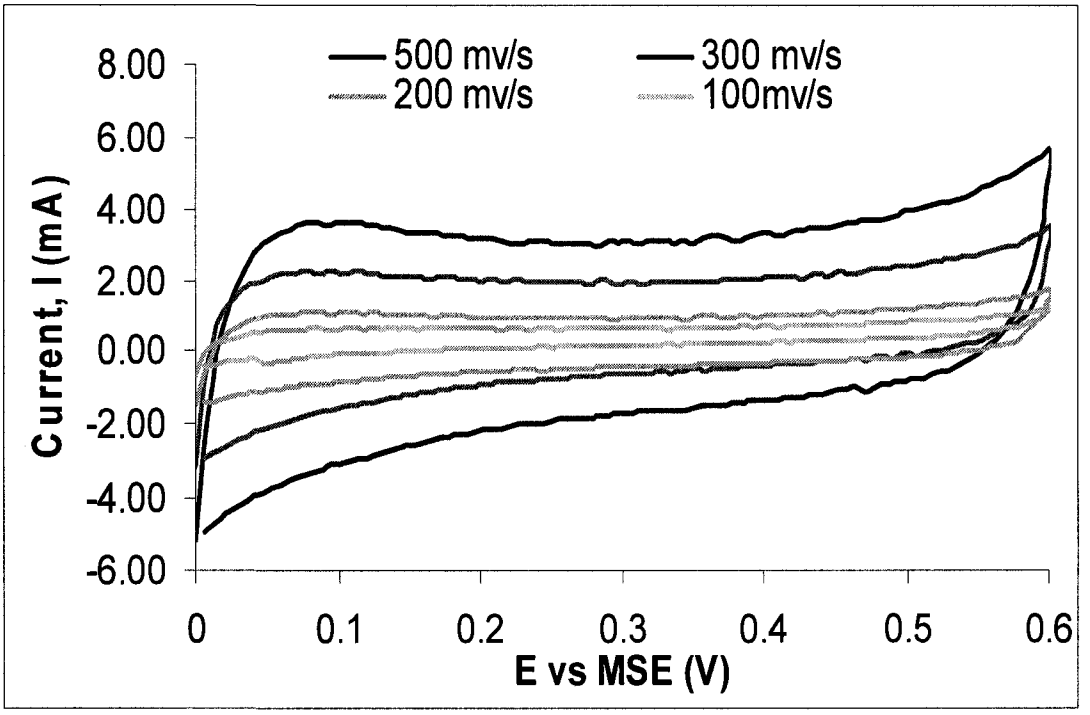

Figure 4.21 CVs of CNT-SS304-400 composite at varying scan rates from 100 mv/s to 500 mv/s

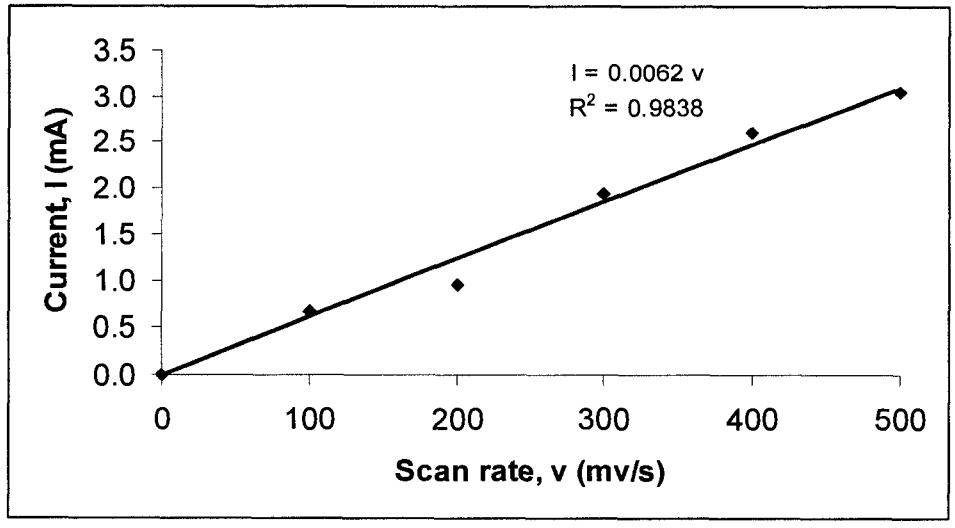

Figure 4.22 Dependence of anodic current at 0.3 V on scan rate of CV for CNT-SS304-400 composite

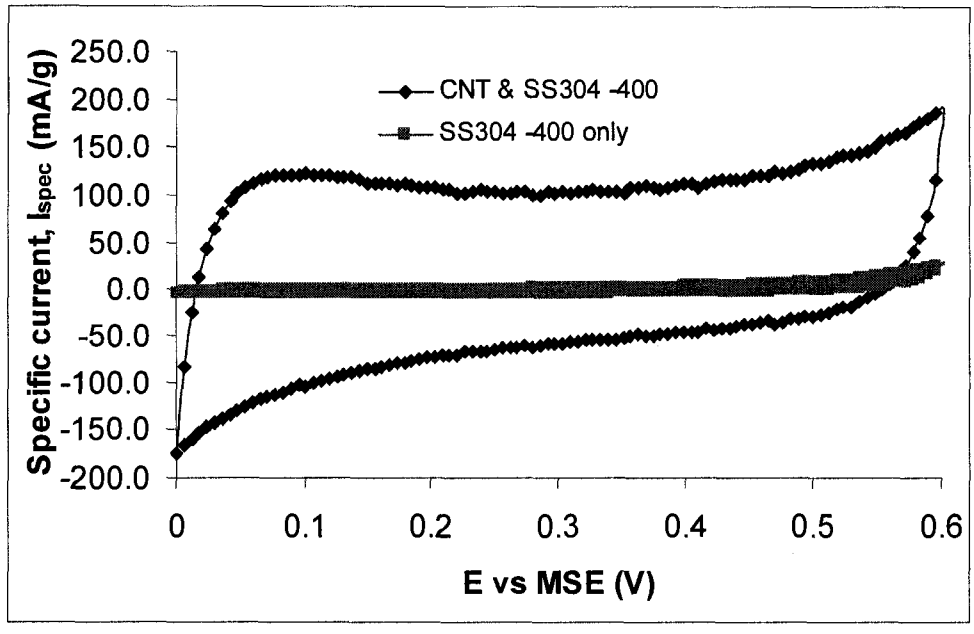

Figure 4.23 Comparison of CVs obtained for blank SS304-400 and CNT-SS304-400 composite at 500mv/s

4.2.4 Summary of electrochemical results

Figure 4.24 compares the three composites studied at a scan rate of 500mv/s. As observed from the CVs for CNT composites with stainless steel grids, higher specific capacitive currents are reached. Looking at Table 4.7, it is seen that the largest total capacitance value is observed for CNT-SS304-40. The total surface area available for electrochemical capacitance is measured to be significantly higher for SS304-40, even

though the specific BET surface area for that composite was lower than that of CNT-SS304-400 since SS304-40 is heavier than SS304-400.

The electrochemically active surface area calculated from the capacitance measurements are found in Table 4.7. Comparing the values obtained in column 6 to column 4, for a gram of any composite material the electrochemically active surface area is slightly less than the BET surface area. This observation is more pronounced for the CNT-SS304-400 composite, where the specific electrochemically active area is approximately 60 % of the specific BET surface area. This ratio is higher for the other samples. This is probably due to the morphology of CNTs. The thick CNT bundles observed for SS304-400 would have smaller pore sizes than the other samples. Thus the electrolyte can only access the available surface area at a certain level. However, since the specific surface area of this composite (SS304-400) is already the largest, the specific electrochemically active surface area would also be larger than the others. In order to validate the effect of porosity, it is necessary to obtain pore size distribution of samples trough a more sophisticated BET surface area analyzer.

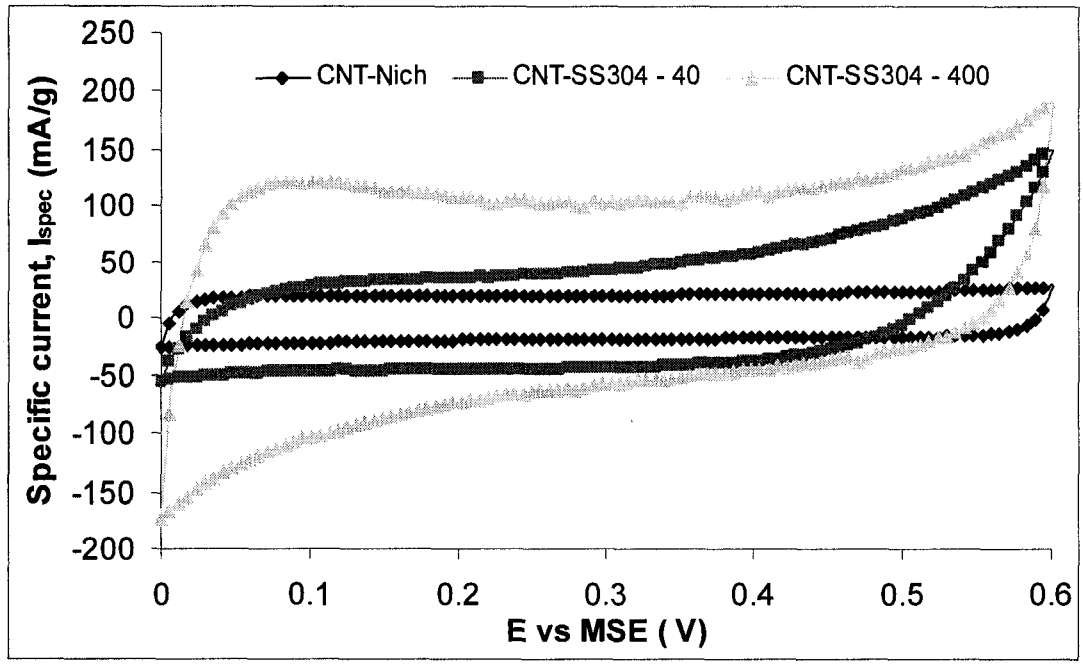

Figure 4.24 Comparison of specific capacitive currents observed for the metallic grids studied.

Table 4.7 Summary of electrochemical results compared to results obtained from BET surface area measurement

Composite	Capacitance [F]	Specific capacitance [F/g]	Specific BET Surface area [m^2/g]	Electrochem. Active Surface Area [cm^2]	Spec. Electrochem. Active Surface Area [m^2/g]
CNT-Nich	0.0071	0.038	0.18	284	0.15
CNT-SS304-40	0.0168	0.095	0.43	672	0.38
CNT-SS304-400	0.0062	0.210	1.32	248	0.84

Another interesting observation is about the relative mechanical strength of the prepared composites. Even though the highest specific capacitance is observed for the CNT-SS304-400 composite, during the measurement of the CV there have been numerous occasions where these composite would break. The failure occurred at the attachment point of the electrode to the alligator clip (Figure 3.2). The smaller wire diameters of these samples would not withstand the corrosive environment of the electrolyte. CNTs synthesized on the metal were not removed even when these samples would break suggesting high strength attachment to the metal. Nich and SS-304-40 composites showed high durability. It was more practical and reliable to obtain CVs for those samples.

Table 4.8 shows the increase in specific capacitance by comparing the values obtained from CV measurements of metallic grids and composites. Even though CNT-SS304-40 has a lower specific capacitance than CNT-SS304-400, when compared to their respective blank cases CNT-SS304-40 show a more significant increase in specific capacitance. The specific capacitance of CNT-SS304-40 is 140 times more than the capacitance of its respective plain metallic grid. When the difference in total capacitance between the plain metallic grid and CNT-metal is divided by the mass of CNTs present, the specific capacitance associated with CNTs only is calculated. The highest specific capacitance for CNTs is achieved for CNT-Nich composites, probably because of the easier wetting of this composite electrode when compared to others. The lack of thick dense bundles for this composite allows for the electrolyte to reach the metal base.

Table 4.8 Comparison of specific capacitance observed for plain metallic grids and their CNT composites

	C_{spec} (F/g)			
Metal	*Plain*	*Composite*	*CNTs*	*Ratio(C_{plain} : $C_{composite}$)*
Nich	0.00055	0.038	12	69
SS304-40	0.00068	0.095	6	140
SS304-400	0.00418	0.21	4	50

Table 4.9 tabulates the specific surface area values obtained by both single point BET surface area and CV measurement for blank metallic grids and their composites as well as theoretical surface areas calculated for blank metallic grids. The specific electrochemically active surface areas measured for the blank metallic grids are considerably lower than those obtained from the BET experiments. However, the specific surface areas of composites for both analysis methods are in agreement. The fact that theoretical calculations are very close to the specific electrochemically active surface areas suggest that the measurement of the surface areas by BET surface area analyzer for materials which have very low surface areas (i.e. metallic grids) will produce erroneous results.

Table 4.9 Comparison of specific surface areas of plain metallic grids and their composites measured by CV and BET and theoretical specific surface areas calculated for plain metallic grids

	S_{Elec}(m^2/g)		S_{BET} (m^2/g)		S_{calc} (m^2/g)
Metal	*Plain*	*Composite*	*Plain*	*Composite*	*Plain*
Nich	2.2×10^{-3}	0.15	0.11	0.18	1.9×10^{-3}
SS304-40	2.7×10^{-3}	0.38	0.17	0.44	2×10^{-3}
SS304-400	1.7×10^{-2}	0.84	0.55	1.32	2×10^{-2}

Chapter 5 : CONCLUSIONS AND RECOMMENDATIONS

5.1 Conclusions

The direct synthesis of CNTs on metal-alloy grids is of great importance to simplify the assembly of CNT electrodes for electrochemical capacitor applications. In this work the CNTs were grown on metallic grids by chemical vapour deposition (CVD) of acetylene (C_2H_2). The metals used were Nichrome (Nich) and stainless steel 304 with 2 mesh sizes of 40 x 40 and 400 x 400 (i.e. S304-40 & SS304-400, respectively). The available iron and nickel in these alloys acted as catalysts for the growth CNTs from. The grids themselves served both as current collectors and as support for CNTs. In addition to the metal-alloy grids, electroless nickel plated copper (ENiCu) was also studied as a substrate to synthesize CNT-metal composites to serve as electrode materials.

Physical characterization of CNT-metal composites by FESEM showed that almost no CNT growth was achieved with ENiCu samples. Higher density of CNTs and yield was observed for SS304 samples. Hydrochloric acid (HCl) treatment of 'as received' samples of SS304-40 showed an increase in amorphous carbon content whereas this treatment increased the yield of CNTs on SS304-400. Thick lengthy bundles of CNTs were synthesized on SS304-400 when the samples were treated in HCl for 2.5 minutes prior to CVD with almost no visible amorphous carbon.

Raman spectroscopy was used to validate the observations made by the FESEM. The purities of the samples in % CNTs were calculated by using the intensities of D and G' peaks. The highest purity of 89 % CNTs was observed for SS304-400 when these samples were treated in HCl for 2.5 minutes prior to CVD. The fact that the CNT purity calculated by this method was lower than the surface coverage values obtained by image analysis, suggested the presence of amorphous carbon embedded in CNT matrix.

Single point BET surface area measurements of plain metallic grids yielded a difference in specific surface areas of at least two orders of magnitude when compared to

the specific theoretical surface areas calculated. Thus, the procedure to determine surface areas of CNTs on metallic grids by BET surface area analysis was inadequate The agreement of surface area values obtained for composite materials by BET analysis and electrochemical experiments as well as the verification of surface area measured for CNT powders by a different BET area analyzer showed that values obtained for composite materials and powders can be trusted but not for plain metallic grids.

Electrochemical performances of CNT-metal composites were investigated by cyclic voltammetry (CV) of the prepared samples in an aqueous environment of 1M sulphuric acid solution. The CNT-Nich composites yielded close to ideal electrochemical capacitor performance but with lower current densities when compared to other composites of CNT-SS304-40 and CNT-SS304-400. Both CNT-SS304-40 and 400 samples showed pseudocapative behaviour. Higher specific capacitance was observed for both CNT-SS304 composites, but SS304-400 samples were mechanically less stable than SS304-400 in the strong acidic environment of the electrolyte.

Compared to their respective plain metallic grids, the highest relative increase in capacitance was observed for CNT-SS304-40. When the difference between the total capacitance of CNT-metal composite and plain metal was normalized by the differential mass (i.e. the mass of CNTs synthesized), the highest specific capacitance of CNTs only was measured for the CNT-Nich sample (12F/g). These were in the same order of magnitude of values obtained by other researchers for unmodified CNT electrodes (10 – 30 F/g). It was surprising that even though SS304-400 samples showed synthesis of thick CNT bundles with higher purity and yield, they did not yield the highest specific capacitance. This was explained by the more difficult wettability of the CNT-SS304-400 composite. Because of the higher yield and densely packed bundles of CNTs observed for this sample, complete wetting of the whole tube structure down to the metal surface was not possible.

5.2 Recommendations

Overall, it is believed by the author of this thesis that it would be more promising to focus on CNT synthesis on Nichrome and SS304-40 rather than SS304-400. Even though these samples yield lower amounts of CNTs, they are easier to manipulate and are more durable. If it is desired to employ an aqueous environment in order to determine electrochemical capacitance of these materials, a method of protecting the metal base from the corrosive environment should be devised. For organic electrolytes, the wetting and corrosion issues can be reduced and higher potential windows can be used (i.e. higher power) but lower ion mobility could be observed. Therefore, it would be important to test the performance of these composites also in organic electrolytes in order to have a better idea about best operating conditions for CNT based composite electrodes to be used as electrochemical capacitors. Once the corrosion effects are resolved, CNT-SS304-400 composites show great promise in terms of electrochemical capacitance. Functionalizing the CNTs synthesized in these composites to make them more hydrophilic would increase their wettability, and thus their specific capacitance. They would also provide the thick CNT background for other types of capacitance enhancement methods such as depositon of transition metal oxides (e.g. RuO) or conducting polymers.

Information on the pore size distribution of the sample is also necessary. When CNTs were densely packed distances between individual tubes would be lowered causing the sample to have a microporous structure. This would increase the specific surface area available but the accessibility of this surface area to the solvated ions in the electrolyte would be reduced, yielding a lower value of specific capacitance. For other samples, especially for CNT-Nichrome, the CNTs were less densely packed and had a lower yield but it was enough to perform as an ideal electrochemical capacitor most probably due to the mesoporous character. These hypotheses need to be verified by analyzing the samples for pore size distribution in a more sophisticated surface area analyzer.

Future researchers in this field should consider using argon instead of nitrogen as a carrier gas to avoid nitridation of metals at high operating temperatures.

REFERENCES

1. Iijima, S., *Helical microtubules of graphitic carbon.* Nature, 1991. **354**: p. 56-58.
2. Popov, V.N., *Carbon Nanotubes : Properties and applications.* Materials Science and Engineering R, 2004. **43**: p. 61-102.
3. Erik T. Thostenson, Z.R., Tsu-Wei Chou, *Advances in the science and technology of carbon nanotubes and their composites: a review.* Composites Science and Technology, 2001. **61**: p. 1899 - 1912.
4. M.S. Dresselhaus, G.D., R.Saito, *Physics of Carbon nanotubes.* Carbon, 1995. **33**(7): p. 883-991.
5. M.-F. Yu, B.S.F., S. Arepalli, R.S. Ruoff, *Tensile loading of ropes of single wall carbon nanotubes and their mechanical properties.* Phys. Rev. Lett. , 2000. **84**(24): p. 5552-5555
6. Yu M., O.L., M.Dyer, K.Moloni, T. Kelly, R.S.Ruoff, *Strength and breaking mechanism of multi walled carbon nanotubes under tensile strength.* Science, 2000. **287**.
7. Ebbesen, T.W., *Carbon nanotubes.* Annual Reviews of Materials Science, 1994. **24**: p. 235-264.
8. L. Dai, A.W.H.M., *Controlled synthesis and modification of carbon nanotubes and C60: carbon nanostructured for advanced polymeric composite materials.* Adv. Mater., 2001. **13**(12-13): p. 899-913.
9. J.-M. Bonard, J.-P.S., T. Stockli, L. Forro, A. Chatelain, *Field emission from carbon nanotubes: perspectives for applications and clues to the emission mechanism.* Appl. Phys. A, 1999. **69**: p. 245 - 254.
10. Jean-Marc Bonard, H.K., Thomas Stockli, Lars-Ola Nilsson, *Field Emission from Carbon nanotubes : the first five years.* Solid-State Electronics, 2000. **45**: p. 893 - 914.
11. J.I. Sohn, S.L., Y.-H. Song, S.-Y. Choi, K.-I. Cho, K.-S. Nam, *Patterned selective growth of carbon nanotubes and large field emission from vertically well-aligned carbon nanotube field emitter arrays.* Appl. Phys. Lett., 2004. **78**: p. 901-903.

12. P. Kim, L.S., A. Majumdar, P.L. McEuen, *Thermal transport measurements of individual multiwalled nanotubes.* Phys. Rev. Lett., 2001. **87**(21): p. 215502-1-4

13. S. Berber, Y.-K.K., D. Tomanek, *Usually high thermal conductivity of carbon nanotubes.* Phys. Rev. Lett., 2000. **84**(20): p. 4613 - 4616

14. M.J. Biercuk, M.C.L., M. Radosavljevic,J.K. Hyun, A.T. Johnson, *Carbon nanotube composites for thermal management.* Appl. Phys. Lett., 2002. **80**(15): p. 2767-2769.

15. T. Guo, P.N., A. Thess, D.T. Colbert, R.E. Smalley, *Catalytic growth of single-walled nanotubes by laser vaporization.* Chem. Phys. Lett., 1995. **243**: p. 49 - 55.

16. R. Andrews, D.J., A.M. Rao, R. Derbyshire, D. Qian, X. Fan, E.C. Dickey, J. Chen, *Continuous production of aligned carbon nanotubes: a step closer to commercial realization,.* Chem. Phys. Lett., 1999. **303**: p. 467 - 474.

17. W.Z. Li, S.S.X., L.X. Qian, B.H. Chang, B.S. Zou, W.Y. Zhou, R.A. Zhao, G. Wang, *Large-scale synthesis of aligned carbon nanotubes.* Science, 1996. **274**: p. 1701-1703.

18. K. Hata, D.N.F., K. Mizuno, T. Namai, M. Yumura, S. Iijima, *Water-assisted highly efficient synthesis of impurity-free single-walled carbon nanotubes.* Science, 2004. **306**: p. 1362-1364.

19. H. Kinoshita, I.K., H. Sakai, M. Tagawa, N. Ohmae, *High growth rate of vertically aligned carbon nanotubes using a plasma shield in microwave plasma-enhanced chemical vapor deposition.* Carbon, 2004. **42**: p. 2753-2756.

20. C. Bower, W.Z., S. Jin, O. Zhou, *Plasma-induced alignment of carbon nanotubes.* Appl. Phys. Lett., 2000. **77**(6): p. 830 - 832.

21. J-M Bonard, H.K., Thomas Stockli, Lars-Ola Nilsson, *Field Emission from Carbon nanotubes : the first five years.* Solid-State Electronics, 2000. **45**: p. 893 - 914.

22. T.Kato, G.H.J., T.Hirata, R. Hatakeyama, *Structure control of carbon nanotubes using radio-frequency plasma enhanced chemical vapor deposition.* Thin solid films, 2004. **457**: p. 2 - 6.

23. N Zhao, C.H., Z. Jiang, J.Li, Y.Li, *Fabrication and growth mechanism of carbon nanotubes by catalytic chemical vapor deposition.* Materials Letters, 2006. **60**: p. 159 - 163.

24. C.J. Lee, J.H.P., J.Park, *Synthesis of bamboo-shaped multiwalled carbon nanotubes using thermal chemical vapor deposition.* Chem. Phys. Lett., 2000. **323**: p. 560-565.

25. S.A. Moshkalyov, A.L.D.M., H.R. Guttierrez, M.A. Cotta, J.W. Swart, *Carbon nanotubes by chemical vapor deposition using thin film nickel catalyst.* Materials science and Engineering B, 2004. **112**: p. 147 - 153.

26. D.Liu, J.C., W.Deng, H. Zhou, Y.Kuang, *Simple catalyst for the direct growth of carbon nanotubes onto substrate by chemical vapor deposition.* Materials Letters, 2004. **58**: p. 2764 - 2767

27. D.Park, Y.H.K., J.K. Lee, *Pretreatment of stainless steel substrate surface for the growth of carbon nanotubes by PECVD.* J.Mat.Sci, 2003. **38**: p. 4933-4939.

28. Y. Saito, T.Y., M. Inagaki, M. Tomita, T. Hayashi, *Growth and structure of graphitic tubules and polyhedral particles in arc-discharge.* Chem. Phys. Lett., 1993. **204**(3,4): p. 277-282

29. D. Zhou, L.C., *Complex structure of carbon nanotubes and their implications for formation mechanism.* J. Appl. Phys, 2003. **93**(12): p. 9972-9976.

30. D.B. Buchholz, S.P.D., R.P.H. Chang, *Mechanism for the growth of multiwalled carbon-nanotubes from carbon black.* Carbon, 2003. **41**: p. 1625 - 1634.

31. S.B. Sinnot, R.A., D.Qian, A.M. Rao, Z.Mao, E.C. Dickey and F. Derbyshire, *Model of carbon nanotube growth through chemical vapor deposition.* Chem. Phys. Lett., 1999. **31 5**.

32. W. Qian, T.L., F. Liu, F. Wei, H. Yuan, *Quantitative Raman characterization of the mixed samples of the single and multi-wall carbon nanotubes.* Carbon, 2003. **41**: p. 1851 - 1854.

33. R.Saito, A.G., Ge G Samsonidze, V. W. Brar, G.Dresselhaus, M.S. Dresselhaus, A.Jorio, L.G. Cancado, C. Fantini, M.A. Pimenta, G. Souza Filho *Double resonance Raman spectroscopy of single-wall carbon nanotubes.* New J. Phys, 2003. **5**: p. 157.1 - 157.15.

34. K.L. Strong, D.P.A., K. Lafdi, J.N. Kuhn, *Purification process for single-wall carbon nanotubes.* Carbon, 2003. **41**: p. 1477 - 1488.

35. R.P. Raffaelle, B.J.L., R.A.DiLeo, *Purity assessment of multiwalled carbon nanotubes by Raman spectroscopy.* J. Appl. Phys, 2007. **101**.

36. S. Brunauer , P.H.E., E.Teller, *Adsorption of gases in multimolecular layers.* Journal of the American Chemical Society 1938. **60**: p. 309-19.

37. R.Kotz, M.C., *Principles and applications of electrochemical capacitors.* Electrochemica Acta, 2000. **45**: p. 2483 - 2498.

38. E. Frackowiak, F.B., *Carbon materials for the electrochemical storage of energy in capacitors.* Carbon, 2001. **39**: p. 937 - 950.

39. D.Qu, H.S., *Studies of activated carbons used in double-layer capacitors.* Journal of Power Sources, 1998. **74**: p. 99 - 107.

40. H.Shi, *Activated carbons and double layer capacitance.* Electrochemica Acta, 1995. **41**(10): p. 1633 - 1639.

41. E.Frackowiak, K.M., V.Bertagna, F.Beguin, *Supercapacitor electrodes from multiwalled carbon nanotubes,* Appl. Phys. Lett., 2000. **77**: p. 2421 - 2423.

42. C. Niu, E.K.S., R.Hoch, D.Moy, H.Tennent, *High power electrochemical capacitors based on carbon nanotube electrodes*, Appl. Phys. Lett., 1997. **70**: p. 1480 -1482.

43. E. Frackowiak, K.Jurewicz, K.Szostak, D.Cazorla-Amoros, F.Beguin, *Enhanced capacitance of carbon nanotubes through chemical activation,* Chem.Phys.Lett, 2002. **361**: p. 35 – 41.

44. E. Frackowiak, K.J., S.Delpeux, F.Beguin, *Nanotubular materials for supercapacitors*, J. Power Sources, 2001: p. 822 - 825.

45. E. Frackowiak , V.K., K. Jurewicz, K.Lota, K.Beguin, *Supercapacitors based on conducting polymers/nanotubes composites,* J.Power Sources 2006. **153**: p. 413 - 418.

46. G. Arabale, D.W., M. Kulkarni, I.S. Mulla, S.P. Vernekar, K. Vijayamohanan, A.M. Rao, *Enhanced supercapacitance of multiwalled carbon nanotubes functionalized with ruthenium oxide,* Chem. Phys. Lett., 2003. **376**: p. 207 - 213.

47. J-K Lee, H.M.P., K-D Jung, O-S Joo, *Electrochemical capacitance of nanocomposite films formed by loading carbon nanotubes with ruthenium oxide* , J. Power Sources, 2006. **159**(1527 - 1531).

48. J Y Lee, K.L., K.H. An, Y.H. Lee, *Nickel oxide/carbon nanotubes nanocomposite for electrochemical capacitance*, Synthetic Metals, 2005. **150**: p. 153 – 157.

49. J.Chen, Z.F., M.Wang, K.Cui, H.Zhou, Y. Kuang, *Preparation and characterization of manganese oxide/CNT composites as supercapacitive materials.* Diamon and Related Materials, 2006. **15**: p. 1478 - 1483.

50. Parthasaradhy, N.V., *Practical Electroplating Handbook.* 1989, New Jersey: Prentice Hall.

51. Reddy, N.K., *Study of growth of Carbon nanotubes on pure metal and metal alloy electrodes*, in *Chemical Engineering.* 2006, McGill University: Montreal.

52. C.J. Alvarez, E. Almanza, L.E. Murr, *Evaluation of the sensitization process in 304 stainless steel strained50% by cold-rolling,* J.Mat. Sci., 2005. **40**: p. 2965 – 2969

53. Baddour, C.E., *Synthesis of CNTs on SS304 strips by Thermal CVD* 2007: Montreal, QC, Canada; McGill University

APPENDIX

Theoretical weight and specific surface area of metallic grids

Mesh sizes are defined as number of openings horizontally and vertically in an inch. The diagram below illustrates the case for a 3 x 3 mesh size. In this case there are 4 wire vertically and 4 wires horizontally. As a general rule :

$N_w = 2(n+1)$; where n is the number of openings in an n x n mesh sized grid and N_w is the number of wires found in an n x n mesh sized grid

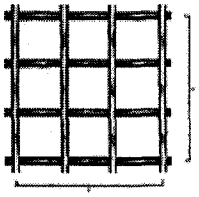

3 x 3 shown here, three openings horizontally and three openings vertically in one inch.

Assuming that wires are perfect cylinders, the weight and specific surface areas of these materials are calculated as follows:

1. Volume of a single wire : $V_w = (\pi D^2 /4) L$, where D is the diameter of the wire and L is the length
2. Volume of 1" x 1" square grid : $V_{grid} = N_w V_w$
3. Weight of 1"x 1" square grid: $W_{grid} = V_{grid} \rho_{metal}$, where ρ_{metal} is the density of the material of construction for the grid
4. Surface area of a single wire : $S_w = 2(\pi D^2 /4) + (\pi D L)$
5. Surface area of 1" x 1" square grid: $S_{grid} = N_w S_w$
6. Specific surface area of the metallic grid : $S_{grid,spec} = S_{grid} / W_{grid}$

	Nich	SS 304-40	SS 304-400
Wire d(inch)	0.01	0.01	0.001
Wire d (m)	0.000254	0.000254	0.0000254
Length (inch)	1	1	1
Length(m)	0.0254	0.0254	0.0254
Nw	82	82	802
Vw (m^3)	1.28×10^{-9}	1.28×10^{-9}	1.28×10^{-11}
Vgrid (m^3)	1.06×10^{-7}	1.06×10^{-7}	1.03×10^{-8}
density (kg/m^3)	8400	8000	8000
Wgrid (kg)	8.87×10^{-4}	8.44×10^{-4}	8.26×10^{-5}
W grid (g)	0.887	0.844	0.0826
Sw (m^2)	2.04×10^{-5}	2.04×10^{-5}	2.03×10^{-6}
Sgrid (m^2)	0.00167	0.00167	0.00163
Sgridspec (m^2/g)	0.00188	0.00197	0.0197